Zika Virus Subverts Stress Granules to Promote and Restrict Viral Gene Expression

Gaston Bonenfant[1], Nina Williams[1], Rachel Netzband[1], Megan C. Schwarz[2], Matthew J. Evans[2] and Cara T. Pager[1]*

[1]Department of Biological Sciences, The RNA Institute, University at Albany-SUNY, Albany, NY 12222

[2]Department of Microbiology, Icahn School of Medicine at Mount Sinai, New York, NY 10029

*Corresponding author:

Cara T. Pager, Ph.D.

Department of Biological Sciences

The RNA Institute

University at Albany-SUNY

1400 Washington Avenue

Albany, NY 12222

Phone: 518.591.8841

Fax: 518.442.4767

E-mail: ctpager@albany.edu

Abstract:

Flaviviruses limit the cell stress response by preventing the formation of stress granules and modulate viral gene expression by subverting different proteins involved in the stress granule pathway. In this study, we investigated the formation of stress granules during Zika virus (ZIKV) infection and the role stress granule proteins play during the viral life cycle. Using immunofluorescence and confocal microscopy, we determined that ZIKV disrupted the formation of arsenite-induced stress granules and changed the subcellular distribution, but not the abundance or integrity, of stress granule proteins. We also investigated the role of different stress granule proteins in ZIKV infection by using target-specific siRNAs to deplete Ataxin2, G3BP1, HuR, TIA-1, TIAR and YB1. Knock-down of TIA-1 and TIAR affected ZIKV protein and RNA levels, but not viral titers. Conversely, depletion of Ataxin2 and YB1 decreased virion production despite having only a small effect on ZIKV protein expression. Notably, however, depletion of G3BP1 and HuR decreased and increased ZIKV gene expression and virion production, respectively. Using an MR766 *Gaussia* luciferase reporter genome together with knockdown and overexpression assays, G3BP1 and HuR were found to modulate ZIKV replication. These data indicate that ZIKV disrupts the formation of stress granules by sequestering stress granule proteins required for replication, where G3BP1 functions to promote ZIKV infection, while HuR exhibits an antiviral effect. The consequence of ZIKV re-localizing and subverting select stress granule proteins might have broader consequences on cellular RNA homeostasis and contribute to cellular gene dysregulation and ZIKV pathogenesis.

22 **Importance:**

23 Many viruses inhibit stress granules (SGs). In this study, we observed that ZIKV restricts SG
24 assembly likely by re-localizing and subverting specific SG proteins to modulate ZIKV replication.
25 This ZIKV-SG protein interaction is interesting, as many SG proteins are also known to function
26 in neuronal granules, which are critical in neural development and function. Moreover,
27 dysregulation of different SG proteins in neurons has been shown to play a role in the progression
28 of neurodegenerative diseases. The likely consequences of ZIKV modulating SG assembly and
29 subverting specific SG proteins are alterations to cellular mRNA transcription, splicing, stability,
30 and translation. Such changes in cellular ribostasis could profoundly affect neural development
31 and contribute to the devastating developmental and neurological anomalies observed following
32 intrauterine ZIKV infection. Our study provides new insights into virus-host interactions and the
33 identification of the SG proteins that may contribute to the unusual pathogenesis associated with
34 this re-emerging arbovirus.

35

36

37 **Introduction:**

38 Zika virus (ZIKV) is an enveloped, single-stranded positive-sense RNA virus belonging to the
39 *Flaviviridae* family, which includes Dengue virus (DENV), Yellow fever virus (YFV), and West Nile
40 virus (WNV) (1). While ZIKV was discovered in Uganda in 1947 (2) , the virus garnered renewed
41 interest during the 2015-2016 outbreak in the Americas (3), in particular because of intrauterine
42 infections and resulting developmental abnormalities such as severe microcephaly, decreased
43 brain tissue, macular scarring, congenital contractures, and hypertonia (4–9). Additionally, adults
44 infected with ZIKV were reported to develop Guillain-Barré syndrome, a debilitating disorder
45 affecting the peripheral nerves (10–13). Similar to other flaviviruses, ZIKV is transmitted by the
46 *Aedes aegypti* and *Aedes albopictus* mosquitoes, although recent evidence has shown ZIKV is
47 also capable of sexual and vertical transmission (14–17). While half a century has passed since
48 the discovery of ZIKV, little-to-no research was published prior to the emergence of the current
49 strain in the Americas associated with devastating developmental pathologies. Because there is
50 no licensed vaccine and antiviral treatments are elusive, a fundamental understanding of the
51 molecular biology of ZIKV and virus-host interactions is critical to developing therapeutic
52 strategies.

53

54 The ZIKV single-stranded positive-sense RNA genome contains a 5'-cap, lacks a poly(A) tail, and
55 encodes one open reading frame (ORF) that is flanked by highly structured 5' and 3' untranslated
56 regions (UTRs). Similar to other flaviviruses, translation of the ZIKV RNA results in one long
57 polyprotein that is co- and post-translationally proteolytically processed to produce at least three
58 structural proteins (capsid [C], premembrane [prM] and envelope [E]) and seven nonstructural
59 proteins (NS1, NS2a, NS2b, NS3, NS4a, NS4b and NS5) (1). Although cap-dependent and cap-
60 independent translation have been reported for DENV (18), it is presently unknown whether ZIKV
61 employs similar translation strategies. Similarly, little is known regarding the strategies ZIKV
62 employs to promote translation of the viral RNA.

63

64 To limit translation of viral RNAs, or protect the cells from different environmental stresses,
65 mammalian cells rapidly stall translation via the activation of one of the four eIF2α kinases. In
66 particular, the presence of double-stranded RNA (dsRNA) during viral infection activates protein
67 kinase R (PKR) (19); the accumulation of unfolded proteins in the endoplasmic reticulum (ER)
68 and resulting stress activates PKR-like endoplasmic reticulum kinase (PERK) (20); amino acid
69 starvation activates general control non-repressed 2 (GCN2) (21); and oxidative stress activates

70 heme-regulated inhibitor kinase (HRI) (22). Phosphorylation of the α subunit of eIF2 by one of
71 the four stress response kinases results in the stalling of translation initiation, and disassembly of
72 polysomes. Stalled translation initiation complexes bound to mRNA are recognized by several
73 RNA binding proteins, which aggregate to form RNA-protein macromolecular complexes called
74 stress granules (SGs) (23). Once the stressor is abated, eIF2α is dephosphorylated by protein
75 phosphatase 1 (PPI) and the PPI cofactor growth arrest and DNA-damage-inducible 34
76 (GADD34), allowing for the return of sequestered mRNA transcripts to active translation (23).
77
78 SGs are dynamic nonmembrane-bound cytoplasmic structures that can rapidly assemble in
79 response to stress and disassemble once the stress has been alleviated (23). SGs typically
80 contain mRNAs, stalled translation initiation complexes, and numerous RNA binding proteins.
81 Indeed, SGs may contain upwards of 260 different proteins (24), and ~50% of these are proposed
82 to be RNA-binding proteins (25). Of these Ras-GTPase activating binding protein 1 (or GAP SH3
83 domain binding protein 1 [G3BP1]), Caprin1, T-cell internal antigen 1 (TIA-1) and TIA-1 related
84 protein (TIAR) are proposed to be key nucleators of SG assembly (26–29). In addition to
85 translation repression and mRNA sorting, SGs also amplify the innate immune response by
86 aggregating critical antiviral factors (23). Because translation is a critical first step in the flavivirus
87 life cycle, the formation of SGs presents an immediate obstacle to infection. Notably, however,
88 during infection with different flaviviruses, such as WNV, DENV, and Japanese encephalitis virus
89 (JEV) SGs are absent, and treatment of virus-infected cells with arsenite fails to induce SGs (30–
90 33). While WNV, DENV and JEV all belong to the same flavivirus genus, each virus employs a
91 unique mechanism to block SG assembly. For example, early during WNV infection PKR is
92 activated by the appearance of exposed dsRNA replication intermediates, which results in
93 phosphorylation of eIF2α, the stalling of translation initiation and formation of stress granules.
94 However, at later times during infection SG formation is limited as membranous vesicles mask
95 dsRNA and viral replication complexes, and thus PKR remains inactive (30, 34, 35). More
96 recently, WNV was shown to also limit SG assembly by upregulating and activating key
97 transcription factors that modulate the antioxidant response (32). In contrast, p38-Mnk1 signaling
98 and phosphorylation of the cap-binding protein eIF4E was affected during DENV infection, thus
99 inhibiting SG formation via an eIF2α phosphorylation-independent mechanism (33). Flaviviruses
100 also subvert specific SG proteins to promote viral gene expression. For example, the SG-
101 nucleating proteins TIA-1 and TIAR facilitate WNV replication (36); G3BP1, G3BP2 and Caprin1

102 promote translation of interferon stimulated genes (ISGs) to limit DENV infection (37, 38); and
103 JEV inhibits SG assembly by co-localizing Caprin1 with the viral capsid protein (31).
104
105 Similar to DENV and WNV, ZIKV was recently shown limit the assembly of SGs (39, 40). In
106 particular, Hou *et al*. reported that exogenously expressed Flag-tagged NS3 and NS4A repressed
107 translation, and the formation of SGs was restricted when Flag-tagged capsid, NS3, NS2B-3 and
108 NS4A proteins were individually expressed (39). Moreover ZIKV RNA was bound by G3BP1, and
109 G3BP1 and Caprin1 co-immunoprecipitated Flag-tagged ZIKV capsid protein (39). Depletion of
110 TIAR, G3BP1 and Caprin1 decreased viral titers, likely as a result of disrupting the interactions
111 with ZIKV capsid protein and RNA (39). Hou *et al*., also showed that SG assembly in ZIKV-
112 infected cells was the consequence of eIF2α phosphorylation and translational repression by
113 activating PKR and the unfolded protein response (39). Amorim et al. additionally reported that
114 ZIKV limits the antiviral stress response by promoting an increase in the rate of eIF2α
115 dephosphorylation during infection (40). While these studies provide insight into how SG
116 formation is inhibited during ZIKV infection, the role of various SG proteins on ZIKV gene
117 expression has yet to be elucidated.
118
119 A number of the RNA-binding proteins that localize in SGs, such as Ataxin-2, G3BP1, HuR and
120 TIA-1, are known to contribute to different neuropathologies (41, 42). Thus, our goal in this study
121 was to investigate the biological impact of different SG proteins linked to neurodegeneration on
122 ZIKV gene expression. Here we show a systematic analysis of SGs during ZIKV infection; the
123 effect of depleting six different SG proteins on ZIKV protein and RNA levels and viral titers; and
124 elucidate the biological function of two SG proteins on ZIKV gene expression. We determined that
125 ZIKV disrupted arsenite-induced SG assembly and that several SG markers co-localized with
126 sites of ZIKV replication. Additionally, the SG protein G3BP1 is required for ZIKV gene expression,
127 while HuR exhibited antiviral activity. Using a MR766 *Gaussia* luciferase reporter genome, our
128 studies revealed that G3BP1 and HuR specifically modulate ZIKV replication. This work advances
129 our understanding of the interplay between ZIKV, the cellular stress response and cellular RNA
130 metabolism, and demonstrates a role for specific RNA-binding proteins in ZIKV replication.
131
132 **Materials and Methods:**
133 *Cell Maintenance and ZIKV Stocks*

134 The hepatocellular carcinoma cell line Huh7 was maintained in Dulbecco's minimal essential
135 medium (DMEM; Life Technologies) supplemented with 10% fetal bovine serum (FBS; Seradigm),
136 10 mM nonessential amino acids (NEAA; Life Technologies), and 5 mM L-glutamine (Life
137 Technologies). Vero cells (ATCC# CRL–81) were maintained in DMEM supplemented with 10%
138 FBS and 10 mM HEPES (Life Technologies). Mammalian cell lines were grown at 37°C with 5%
139 CO_2. C6/36 cells (ATCC# CRL-1660) grown at 27°C with 5% CO_2 were maintained in Eagle's
140 minimal essential medium (EMEM; Sigma) supplemented in 10% FBS, sodium pyruvate (0.055
141 g/L; Life Technologies), Fungizone (125 µg/L; Life Technologies), and penicillin and streptomycin
142 (50000 units/L penicillin, 0.05 g/L streptomycin; Life Technologies). ZIKV (Cambodia-160310,
143 Uganda MR766, and Puerto Rico PRVABC59; generous gifts from Dr. Brett Lindenbach, Yale
144 School of Medicine; Dr. Laura Kramer, Wadsworth Center NYDOH; and the CDC) stocks were
145 generated in C6/36 cells. Briefly, C6/36 cells nearing confluency were infected at a multiplicity of
146 infection (MOI) of 0.1. Seven days post-infection supernatants from the infected cells were
147 collected, aliquoted and stored at -80°C. RNA was extracted from cells to confirm infection via
148 northern blotting, and viral titers were determined by plaque assay.
149
150 *Small Interfering RNA (siRNA) and DNA Plasmid Transfections*
151 Sense and antisense siRNA oligonucleotides were synthesized by Integrated DNA Technologies
152 (IDT). The siRNA sequences are provided in Table 1. Oligonucleotides were resuspended in
153 RNase-free water to a 50 µM final concentration. Sense and antisense strands were combined in
154 annealing buffer (150 mM HEPES (pH 7.4), 500 mM potassium acetate, and 10 mM magnesium
155 acetate) to a final concentration of 20 µM, denatured for 1 minute at 95°C, and annealed for 1
156 hour at 37°C (43).
157
158 For siRNA and plasmid transfections, Huh7 cells seeded at $7.5x10^6$ in a 10 cm cell culture dish
159 were transfected 24 hours later with 100 nM of the indicated siRNA duplex or 2 µg of 3xFLAG-
160 BAP (Bacterial Alkaline Phosphatase; Sigma #C7472), HuR-Flag (GenScript #OHu23723D), or
161 G3BP1-Flag (GenScript #OHu02150D) plasmids using Lipofectamine 3000 (Invitrogen) per
162 manufacturer's protocol. At 24 hours post-transfection, cells were infected with ZIKV.
163
164
165

166 **Table 1: siRNA Sequences**

Target	Sense-Strand (5'-3')	Antisense-Strand (5'-3')
Ataxin-2	AAGUGUGAUUUGGUACUUGAU	UGAAGGGUGCGUCAUAUAGGG
G3BP1	CAGGAAGACUUGAGGACAUUU	AUGUCCUCAAGUCUUCCUGUU
GL2	CGUACGCGGAAUACUUCGAUU	UCGAAGUAUUCCGCGUACGUU
HuR	AAGAGGCAAUUACCAGUUUCAUU	UGAAACUGGUAAUUGCCUCUUUU
TIA-1	CUGGGCUAACAGAACAACUAAUU	UUAGUUGUUCUGUUAGCCCAGUU
TIAR	AAGGGCUAUUCAUUUGUCAGAUU	UCUGACAAAUGAAUAGCCCUUUU
YB1	GGCAGCAAAUGUUACAGGUtt	ACCUGUAACAUUUGCUGCCtc

167

168 *ZIKV Infections*

169 On the day of infection, one mock culture plate was trypsinized and counted to calculate MOI.
170 Cells were infected at either MOI of 1 or 5, as noted in the text and figure legends. Appropriate
171 amount of viral stocks thawed at room temperature were diluted in PBS to a final volume of 3.5
172 mL. Culture dishes were aspirated, the viral solution was added, and cells were returned to the
173 incubator for 1 hour with rocking every 15 minutes. At the end of the hour 4 mL complete media
174 was added to each plate.

175

176 *Immunofluorescence Analysis and Confocal Microscopy*

177 Cells seeded in 8-chambered slides (Nunc Lab-Tek Chamber Slide system; Sigma C7182) were
178 infected with ZIKV at MOI of 5. Two days post-infection, cells were either mock-treated or treated
179 with sodium arsenite (1 mM final concentration; Sigma) for 30 minutes. Hereafter the cells were
180 washed three times with phosphate-buffered saline (PBS) and fixed with paraformaldehyde (4%)-
181 PBS for 10 minutes at room temperature. Cells were washed once with PBS and permeabilized
182 with 100% ice-cold methanol for 15 minutes at room temperature. Cells were washed in blocking
183 buffer (PBS-1% fish gelatin (FG); Sigma) three times for 15 minutes. Primary antibody was diluted
184 in blocking buffer, added to the appropriate wells and incubated overnight at 4°C. Secondary
185 antibodies diluted in blocking buffer were added for 1 hour at room temperature in the dark.
186 Hoechst-33342 (Life Technologies) was applied for 15 minutes. Between and after application of
187 antibodies, cells were washed with blocking buffer three times for 15 minutes. Finally, the cells
188 were washed twice with PBS for 5 minutes, the 8-chamber upper structure was removed,
189 Fluoromount (Southern Biotech) added, and a cover-slip applied. Slides were stored at 4°C if
190 imaging was undertaken within 1 week, or at -20°C for long-term storage. Antibodies and

191 concentrations used are listed in Table 2. Slides were imaged on a Zeiss LM710 confocal
192 microscope with a 63x oil objective.
193
194 **Table 2: Antibodies and Concentrations**

Protein	Supplier (Product ID)	Species	IFA Dilution	Western Dilution
G3BP1	Bethyl (A302-034A)	Rabbit	1:300	1:5,000
TIAR	Bethyl (A303-613A)	Rabbit	1:250	1:1,000
YB1	Cell Signaling (D299)	Rabbit	1:250	N/A
Ataxin-2	ProteinTech (21776-1-AP)	Rabbit	1:200	1:5,000
HuR	ProteinTech (11910-1-AP)	Rabbit	1:200	1:6,000
YB1	Novus (NBP1-97572)	Rabbit	N/A	1:5,000
TIA-1 (C-20)	Santa Cruz (Sc-1751)	Goat	1:50	1:3,000
eIF3	Santa Cruz (Sc-16377)	Goat	1:50	N/A
GRP78	Santa Cruz (Sc-376768)	Goat	N/A	1:1,000
Fibrillarin	ProteinTech(16021-1-AP)	Rabbit	N/A	1:5,000
Calnexin	ProteinTech (10427-1-AP)	Rabbit	N/A	1:5,000
GAPDH	Millipore Sigma	Mouse	N/A	1:10,000
ZIKV Capsid	GeneTex (GTX133317)	Rabbit	N/A	1:5,000
ZIKV Envelope	BioFront (1176-76)	Mouse	1:800	N/A
ZIKV NS5	BioFront (6A1)	Mouse	1:150	N/A
Anti-rabbit-peroxidase	Santa Cruz (Sc-2313)	Donkey	N/A	1:10,000
Anti-goat-peroxidase	Santa Cruz (Sc-2354)	Mouse	N/A	1:5,000
Anti-mouse-peroxidase	Santa Cruz (Sc-2314)	Donkey	N/A	1:10,000
Anti-mouse-488	Life Technologies	Donkey	N/A	1:200
Anti-rabbit-594	Life Technologies	Donkey	N/A	1:200
Anti-goat-647	Life Technologies	Donkey	N/A	1:200

195 *N/A Not applicable
196
197 *Quantification of SG-positive Cells*
198 A 40x oil objective was used to acquire images of ZIKV-infected cells stained with mouse-anti-
199 dsRNA antibody to detect ZIKV-infected cells and one of the following anti-SG protein antibodies:
200 rabbit-anti-Ataxin-2, rabbit-anti-G3BP1, rabbit-anti-HuR, goat-anti-TIA-1, rabbit-anti-TIAR, and
201 rabbit-anti-YB1. To quantify the effect of ZIKV infection on SG formation, 200 to 300 infected cells
202 between three or more biological replicates were counted. Quantification of SGs between different
203 infections was completed as follows: for each treatment, the percentage of uninfected cells
204 with/without SGs and ZIKV-infected cells with/without SGs was calculated. Using the percentages

205 from cells with/without SGs from three or more biological replicates, a one-tailed student T-test
206 was carried out.
207
208 *Subcellular Fractionation*
209 Huh7 cells seeded in 10 cm cell culture dishes at $7.5x10^6$ were infected at a MOI of 5. Two days
210 post-infection, the cells were trypsinized, centrifuged at 500 x g for 5 minutes, and resuspended
211 in PBS. Cytoplasmic and nuclear proteins were separated using the NE-PER extraction reagents
212 per manufacturer's protocol (ThermoScientific). After clarification of proteins, 30 μg of protein
213 lysate from the cytoplasmic and nuclear fractions were analyzed by western blot analysis. To
214 demonstrate successful separation of cytoplasmic and nuclear fractions the western blots were
215 also probed for the ER chaperone protein GRP78 and Fibrillarin, a methyltransferase enzyme
216 that 2'O-methylates ribosomal RNA, respectively. Quantification of band intensities was
217 performed using Image Lab software (BioRad). The subcellular distribution of SG proteins in
218 ZIKV-infected cells was normalized to the corresponding mock-infected lane, and an average of
219 three independent experiments was used to generate the quantification graph.
220
221 *Harvest of ZIKV-Infected Cells for Protein and RNA Analysis*
222 At the indicated time point, media from culture dishes was aspirated and the cells were washed
223 once with PBS. Cells were manually scraped from plate in 1 mL PBS, divided between two
224 microcentrifuge tubes, and pelleted at 14,000 RPM for 15 seconds. The supernatant was
225 removed, and cells were resuspended in 50 μL RIPA buffer (100 mM Tris-HCl (pH 7.4), 150 mM
226 NaCl, 1% sodium deoxycholic acid, 1% Triton-X100, 0.1% SDS) containing protease inhibitors
227 (mini tablets EDTA-free; ThermoScientific Pierce) or 1 mL TRIzol (Invitrogen) for protein and RNA
228 analysis, respectively. For protein analysis, cells resuspended in RIPA buffer with protease
229 inhibitors were incubated on ice for 20 minutes. The lysate was clarified by centrifugation at
230 14,000 RPM at 4°C for 20 minutes. The clarified protein lysate was collected and processed for
231 western blot analysis. RNA from cell lysates was extracted using TRIzol per the manufacturer's
232 instructions.
233
234 *Western Blot Analysis*
235 Protein lysates were quantified using the DC protein assay kit (BioRad) and 20 μg lysate was
236 electrophoresed for 2 hours at 100V through SDS-10% PAGE. Protein was transferred to a PVDF

237 membrane at 100 V for 60 minutes at 4°C. Transfer efficiency was determined by Ponceau S
238 (Sigma) staining, after which the blots were washed in buffer (0.1% Tween in PBS (PBS-T)) and
239 blocked for 30 minutes in blocking buffer (5% powdered milk (w/v) in PBS-T). Primary antibodies
240 diluted in blocking buffer were added to the blots and incubated at 4°C overnight. Secondary
241 antibodies diluted in blocking buffer were incubated at room temperature for 1 hour. The assay
242 was developed using Clarity Western ECL Blotting Substrate (BioRad) and imaged on a
243 chemiluminescent imager (BioRad). Prior to application of additional antibody, blots were stripped
244 using ReBlot Plus Mild (Millipore Sigma) according to manufacturer's suggestion. Before and after
245 application of primary/secondary antibodies and stripping, blots were washed for 15 minutes three
246 times in wash buffer. Antibodies and concentrations are listed in Table 2.
247
248 *Northern Blot Analysis*
249 TRIzol-extracted RNA (10 µg) was resuspended in loading buffer (1x MOPS-EDTA-sodium
250 acetate (MESA; Sigma), 4.5% formaldehyde, and 32% formamide), denatured for 15 minutes at
251 65°C, separated in a 1.2% agarose gel containing 5.92% formaldehyde (v/v) and 1x MESA (v/v),
252 and transferred via capillary action to a Zeta-probe membrane (BioRad) overnight at room
253 temperature. RNA was crosslinked to the membrane using a TL-2000 (UVP) and then stained
254 with methylene blue to visualize transfer of RNA. Methylene blue was removed by washing the
255 membranes in 1xSSC/1% SDS for 15 minutes three times, and then prehybridized in 5 mL
256 ExpressHyb (ClonTech) for 1 hour at 65°C. The hybridization buffer was changed and a ^{32}P-
257 labeled dsDNA probe (Invitrogen) was added for 1 hour at 65°C. Blots were then washed with
258 0.1xSSC/0.1% SDS three times for 15 minutes at 55°C, exposed overnight to a phosphorimager
259 screen, and subsequently visualized on a Typhoon 9400 (GE). The ZIKV 3' UTR probe (targeting
260 nt 10324-10808 of the viral genome) was generated by RT-PCR amplification of the 3' UTR region
261 from ZIKV-infected cells and the resulting PCR product cloned into pCR-TOPO2.1 (Invitrogen).
262 The actin and ZIKV probes were randomly labeled with α^{32}P dATP (Perkin Elmer) using a
263 RadPrime labeling kit (Invitrogen).
264
265 *Isolation of ZIKV Replication Complexes*
266 A protocol adapted from Schlegel *et al.*, and Chen *et al.*, was used to isolate ZIKV replication
267 complexes (44, 45). Huh7 cells seeded in 15 cm cell culture dishes were either mock-infected or
268 infected with ZIKV (Cambodia-160310) at a MOI of 1 and then harvested 1-day post-infection.

269 Specifically, cells were washed twice with cold PBS, gently dislodged using a cell lifter, collected
270 and pelleted at 1,000 RPM for 5 minutes at 4°C. The cell pellets were resuspended in 1 mL
271 hypotonic buffer (10 mM Tris-HCl [pH 8.0], 10 mM NaCl, 1 mM $MgCl_2$) containing protease and
272 phosphatase inhibitors (mini tablets EDTA-free; ThermoScientific Pierce). One-tenth volume of
273 cells (100 μL) was collected for the protein input sample, which was lysed in RIPA buffer as
274 described above. The cells in hypotonic buffer were incubated on ice for 10 minutes. After
275 incubation, cells were homogenized using the tight pestle of a Dounce homogenizer
276 approximately 50 times on ice. Samples were then centrifuged at 1,000 x g for 10 minutes at 4°C,
277 the supernatant collected and NaCl was added to the supernatants to a final concentration of 300
278 mM. The replication complexes in the collected supernatant were separated in a 10%/60%
279 gradient. The 10%/60% sucrose gradient was prepared in Ultraclear tubes (Beckman Coulter) by
280 first adding 5.5 mL of 10% sucrose solution (300 mM NaCl, 15 mM Tris-HCl [pH 7.5], 15 mM
281 $MgCl_2$, and 10% sucrose), followed by a slow deposition of 5.5 mL 60% sucrose (300 mM NaCl,
282 15 mM Tris-HCl [pH 7.5], 15 mM $MgCl_2$, and 60% sucrose) below the 10% sucrose layer. Samples
283 were layered onto the sucrose gradients and ultracentrifuged using the SW41 rotor at 26,000
284 RPM for 16 hours at 4°C. The opaque layer sedimenting between the 10% and 60% sucrose
285 layers was collected for analysis. For western blot analysis the proteins were precipitated with
286 methanol and resuspended in a buffer containing 8 M urea and 100 mM Tris-HCl (pH 8.0).
287
288 *Plaque Assays*
289 Six-well plates were seeded with $6x10^5$ Vero cells per well. The following day, serial dilutions of
290 virus were prepared in PBS, media was aspirated, and 300 µL of appropriate dilution was added.
291 Cultures were returned to incubator for 1 hour with rocking every 15 min. After incubation, 2.5 mL
292 of a 1:1 overlay (1.2% Oxoid agar and modified media (2xDMEM, 4% FBS, 10 mM HEPES) was
293 added to each well. Agar was left to solidify at room temperature for 10 minutes before returning
294 the plates to incubator. At 4 days post-infection, plaques were developed using 1% crystal violet
295 in 20% methanol.
296
297 *Cell Viability Assays*
298 Huh7 cells seeded at $5x10^5$ in a 6 cm cell culture dish were transfected 24 hours later with the
299 indicated siRNA duplex using Lipofectamine 3000 (Invitrogen) as per manufacturer's protocol.
300 After 24 hours, cells were trypsinized and seeded in triplicate into a white 96-well plate. Forty-

301 eight hours after seeding the multi-well plate, the original 6 cm culture dish was harvested for
302 protein to confirm knockdown, and a cell viability assay was performed. An equal volume of
303 CellTiter-Glo 2.0 (100 µL; Promega) to cell culture media was added to each well, which was
304 rocked for two minutes following a ten-minute room temperature incubation. Luminescence was
305 recorded with an integration time of one second using a BioTEK Synergy luminometer.
306
307 *Luciferase Reporter Virus and Assays*
308 To construct a ZIKV reporter virus, the *Gaussia* luciferase gene was cloned as a fusion with the
309 amino terminus of the polyprotein, as previously described for another ZIKV strain (46), into the
310 previously described plasmid pCDNA6.2 MR766 Intron3127 HDVr encoding a CMV promoter
311 driven MR766 ZIKV (47). Specifically, a translational fusion was generated comprised of the first
312 20 amino acids of the Capsid protein, the full-length *Gaussia* luciferase reporter gene, along with
313 its signal sequence, the FMDV 2A peptide, and finally the full-length viral polyprotein. The
314 flavivirus cyclization sequence determinants in full length capsid coding region was disrupted by
315 silent mutagenesis (indicated here by lower case nucleotides: 5' ATT GTa AAc ATG tTA AAA) To
316 create a replication incompetent version of this plasmid, this reporter cassette was also cloned
317 into the previously described pCDNA6.2 MR766 Intron3127 Pol(-) HDVr (47) to create pCDNA6.2
318 MR766 clGLuc Intron3127 Pol(-) HDVr.
319
320 Huh7 cells were seeded into 6 cm cell culture dishes at a density of $5x10^5$ cells/dish. For siRNA
321 experiments, the cells were transfected with siRNAs 24-hours after seeding of the cells. Twenty-
322 four hours post-transfection, cells were subsequently seeded into 24-well plates at a density of
323 $5x10^4$ cells/well. The following day, 200 ng of the replication-competent and replication-
324 incompetent pCDNA6.2 MR766 clGLuc Intron3127 HDVr, along with appropriate siRNAs (40 nM)
325 or plasmid DNA (500 ng) were transfected using Lipofectamine 3000. At 6, 24, 48- and 96-hours
326 post-transfection, media from wells was collected and stored at -20°C. Assays were performed
327 using NEB BioLux *Gaussia* Luciferase (GLuc) kit (NEB #E3300L) following the stabilized protocol.
328 Briefly, samples and GLuc assay solution were prepared and equilibrated to room temperature.
329 The sample (35 µL) was added to three individual wells in a white 96-well plate. The GLuc assay
330 solution (50 µL) was dispensed into each sample well, shaken for 5 seconds, incubated at room
331 temperature for 30 seconds, and luminescence recorded with an integration time of 10 seconds
332 using a BioTEK Synergy luminometer.
333

334 *Statistical Analysis*

335 For RNA quantification of northern blots, ImageQuantTL was used to obtain the mean density of
336 gZIKV, sgZIKV, and actin RNA. RNA levels of ZIKV were initially divided by the mean density of
337 actin and subsequently standardized to the control siGL2 (or 3xFlag-BAP). A two-tailed student
338 T-test comparing control RNA levels to each knockdown (or overexpression) sample was
339 performed using data from three or more biological replicates. Relative viral titers were
340 determined by standardizing the plaque forming units/mL (PFU/mL) for each treatment to the
341 control siRNA (siGL2) or plasmid (p3xFLAG-BAP). A two-tailed student T-test was performed
342 using relative viral titers from three biological replicates. All graphs were generated using
343 Microsoft Excel for Mac 2011. Statistical analysis was performed using StatPlus:mac LE.

344

345

346 **Results:**

347 **ZIKV inhibits arsenite-induced SG formation.** To determine whether SGs form during ZIKV
348 infection, Huh7 cells were infected with the Cambodian-isolate (160310) at an MOI of 5, and the
349 formation of SGs at 24 hours post-infection was visualized by immunofluorescence and confocal
350 microscopy using an antibody to detect TIA-1, a protein known to facilitate nucleation of SGs (27).
351 ZIKV-infected cells were identified by staining for double-stranded (ds) RNA, a marker of viral
352 replication sites. In mock-infected cells, TIA-1 localized to the nucleus (Figure 1A). Similar to other
353 flavivirus infected cells (30, 31), TIA-1 was mostly localized in the nucleus and we observed ~10%
354 of ZIKV-infected cells containing SG foci in the cytoplasm (Figure 1A and Figure 1C). A lack of
355 SGs during ZIKV-infection suggested ZIKV either inhibited the formation of SGs or promoted the
356 disassembly of SGs. To investigate whether ZIKV inhibited the formation of SGs, we treated cells
357 with 1 mM sodium arsenite for 30 minutes. In mock-infected cells treated with sodium arsenite,
358 we observed 80-100% of the cells containing TIA-1 SGs in the cytoplasm (Figure 1). In contrast,
359 TIA-1-containing SGs were observed in ~24% of ZIKV-infected treated with sodium arsenite
360 (Figure 1B and Figure 1D).

361

362 We similarly investigated SG formation following infection with the 1947 Uganda-isolate (MR766)
363 and a recent ZIKV strain isolated in Puerto Rico in 2015 (PRVABC59) (44, 45). Similar to Huh7
364 cells infected with the Cambodia-ZIKV strain (Figure 1C), ~10% of cells infected with MR766 or
365 PRVABC59, had TIA-1-containing SGs (Figure 1E and Figure 1G). Consistent with the number
366 of SGs in cells infected with the Cambodia ZIKV strain (Figure 1D), approximately 20% of cells

367 infected with MR766 or PRVABC formed TIA-1-SGs following treatment with sodium arsenite
368 (Figure 1F and Figure 1H). These data indicate that the three ZIKV strains (Cambodia, Uganda
369 and Puerto Rico) examined restrict the formation of SGs when treated with sodium arsenite and
370 are consistent with SG studies undertaken with WNV, DENV and ZIKV (30, 32, 33, 39, 40).
371
372 To determine whether ZIKV inhibited a particular subset of SGs, we next investigated the
373 formation of SGs containing Ataxin-2, G3BP1, eIF3B, HuR, TIAR, and YB1 in mock and ZIKV
374 (Cambodia-160310)-infected cells in the absence or presence of sodium arsenite (Figure 1C and
375 Figure 1D). Quantification of the different SG proteins in mock-infected cells showed that less
376 than 10% of untreated cells contained SGs, while SGs were visible in more than 90% of cells
377 treated with sodium arsenite (Figure 1C and Figure 1D). In contrast, analysis of SGs as visualized
378 using the different SG proteins in cells infected with the Cambodia ZIKV-isolate (160310), showed
379 that 1-25% of untreated cells and 18-56% of sodium arsenite-treated contained SGs (Figure 1C
380 and Figure 1D). We noted that a significant number of ZIKV-infected cells formed Ataxin-2 and
381 YB1 containing SGs in untreated cells, and that the number of cells with SGs containing YB1
382 increased following sodium arsenite-treatment. Overall, ~20% of ZIKV-infected cells showed
383 sodium arsenite-induced SGs containing common SG components (Figure 1D, Figure 1F and
384 Figure 1H). However, we also observed that 44% of infected cells showed SGs containing the
385 translation initiation factor eIF3B (Figure 1D, Figure 1F and Figure 1H), indicating that the SGs
386 induced in ZIKV-infected cells contain translationally repressed ribonucleoprotein complexes.
387 Together these data show that all three ZIKV strains inhibit the formation of SGs albeit to different
388 extents.
389
390 **ZIKV does not dramatically change the abundance or integrity of SG proteins during**
391 **infection.** To determine if the ability of ZIKV to inhibit sodium arsenite-induced SG assembly is a
392 result of promoting proteolytic cleavage of and/or degrading SG-nucleating proteins, we infected
393 Huh7 cells with ZIKV at a MOI of 1 and 5 and investigated the abundance and integrity of select
394 SG proteins at 1, 2, and 3 days post-infection. By western blot analysis we found that the
395 abundance of most SG proteins remained the same between mock- and Cambodia ZIKV-infected
396 samples (Figure 2A), and no cleavage products were identified (Figure 2A and Figure 2B).
397 Interestingly, independent of MOI, the levels of Ataxin-2 increased with ZIKV infection at 1- and
398 2-days post-infection (Figure 2A). We similarly observed an increase in Ataxin-2 abundance and
399 no change in HuR, TIA-1 and TIAR levels following infections with the Ugandan and Puerto Rican

400 strains (Figure 2B). We also observed a modest decrease in G3BP1 levels (Figure 2A and Figure
401 2B). While Poliovirus 3C protease has been shown to cleave G3BP1 and block the formation of
402 SGs, we did not observe such a cleavage product (48). It is possible that G3BP1 was cleaved
403 during ZIKV-infection, however the modest decrease in G3BP1 levels likely limited the detection
404 of such a fragment by western blot analysis. Alternatively, G3BP1 might be degraded during ZIKV-
405 infection. Thus, the ability of ZIKV to block the assembly of stress granules was not the result of
406 a change in the abundance or proteolytic cleavage of HuR, TIA-1, and TIAR. However, changes
407 in Ataxin-2 and G3BP1 levels might in part restrict the formation of SGs during ZIKV infection.
408
409 **SG proteins are re-localized during ZIKV infection.** To investigate whether SG proteins are re-
410 localized during ZIKV infection, we examined the relative distribution of different SG markers in
411 the cytoplasm versus nucleus. In particular, Huh7 cells were either mock- or ZIKV-infected at a
412 MOI of 5, and 1-day post-infection the cytoplasmic and nuclear fractions were isolated and the
413 subcellular distribution of Ataxin-2, G3BP1, HuR, TIA-1, TIAR, and YB1 analyzed by western blot
414 (Figure 2C). To demonstrate effective isolation of the cytoplasmic and nuclear fractions, and to
415 show standardization of the amount of loaded proteins, we examined the localization and
416 abundance of GRP78 (or BiP), an endoplasmic reticulum chaperone protein, and Fibrillarin, the
417 methyltransferase protein that 2'O-methylates ribosomal RNA and is localized in the nucleoli.
418 Western blot detection of ZIKV NS5 confirmed infection, and consistent with immunofluorescence
419 studies (Figure 6A; (49)) showed that ZIKV NS5 was predominantly localized in the nuclear
420 fraction. We semi-quantified the amount of the respective SG protein in each fraction by
421 normalizing the band intensities in the cytoplasmic and nuclear fractions to GRP78 and Fibrillarin,
422 respectively. Normalized values were then standardized to mock samples to obtain a relative
423 change in distribution of each protein. Thus, the ratio of band intensities less-than-one indicate a
424 decrease in the respective fraction, while values greater-than-one represent an enrichment of the
425 SG protein in the subcellular fraction (Figure 2D and Figure 2E). Overall, we did not observe
426 differences in the distribution of Ataxin-2, G3BP1, TIA-1, TIAR and YB-1 between the cytoplasmic
427 and nuclear fractions (Figure 2D and Figure 2E). In contrast however, the relative abundance of
428 HuR in the nuclear fraction decreased, and the concomitant amount of HuR in the cytoplasm
429 increased (Figure 2D and Figure 2E). Indeed, immunofluorescence analysis of HuR localization
430 in mock- and ZIKV-infected cells showed strong nuclear staining, and increased staining in the
431 cytoplasm in ZIKV-infected cells (Figure 5B). We also quantified the fluorescence signal from
432 confocal microscopy images by examining HuR localization in mock- and ZIKV-infected cells. In

433 particular, the fluorescence signal in confocal microscopy images of HuR in the nucleus was
434 quantified. The relative fluorescence intensity signal of HuR, in mock-infected cells was arbitrarily
435 set to 1 (Figure 2F). Using this quantification analysis, a value greater-than-one would indicate
436 increased nuclear localization, and a value less-than-one would indicate decreased localization
437 in the nucleus. Similar to the subcellular fractionation and western blot analysis, we observed a
438 decreased amount of HuR protein in the nucleus in ZIKV-infected cells compared to mock-
439 infected cells (Figure 2E and Figure 2F). These data together show that the subcellular
440 localization of most SG proteins does not significantly change during ZIKV infection. In contrast,
441 however HuR is re-distributed from the nucleus into the cytoplasm in ZIKV-infected cells. That SG
442 proteins, particularly those that promote SG-assembly, do not significantly accumulate in the
443 cytoplasm may in part contribute to the reduction in the number of SGs during ZIKV infection.
444
445 **G3BP1 and HuR modulate ZIKV gene expression.** To elucidate the role of SG proteins during
446 ZIKV infection we transfected Huh7 cells with siRNAs targeting six different SG proteins and
447 infected with the Cambodian-isolate (160310) at a MOI of 5. Two days post-infection cells were
448 harvested for protein and RNA analysis by western and northern blot, and media was collected
449 for plaque assays. Western blot analysis from at least three independent experiments, showed
450 that the siRNAs effectively depleted the abundance of the targeted SG proteins (Figure 3A). For
451 the majority of the SG proteins examined, siRNA depletion of the individual SG proteins did not
452 impact the levels of other SG markers. We did however observe that the levels of TIA-1 modestly
453 decreased following knockdown of HuR (Figure 3A). TIA-1 levels have similarly been shown to
454 be modulated in cells deficient in another cellular RNA binding protein, namely TIAR (36). In
455 examining the effect of SG protein depletion on ZIKV, the abundance of the ZIKV capsid protein
456 (Figure 3A) did not change following depletion of Ataxin-2. We did however observe a dramatic
457 decrease in viral protein when G3BP1 was depleted, while knockdown of HuR and TIA-1
458 substantially increased ZIKV capsid protein levels (Figure 3A). Depletion of TIAR and YB1
459 similarly increased the amount of ZIKV capsid protein, albeit not to the same extent as depletion
460 of HuR and TIA-1 (Figure 3A).
461
462 We next examined the abundance of ZIKV genomic RNA (gRNA). By northern blot we observed
463 significant reductions in gZIKV levels following depletion of G3BP1 compared to cells transfected
464 with the control siRNA, siGL2 (Figure 3B). Depletion of Ataxin-2, TIAR and YB1 also decreased
465 gZIKV (Figure 3B). Depletion of TIA-1 did not significantly affect the levels of viral RNA (Figure

466 3B). Consistent with the increase in ZIKV capsid protein, depletion of HuR significantly increased
467 gZIKV levels (Figure 3B). During flaviviral infections incomplete degradation of the viral gRNA by
468 the cellular 5'-to-3' exonuclease Xrn1 produces a small noncoding viral RNA or subgenomic
469 flavivirus RNA (sfRNA) that corresponds to the 3' UTR (50). In our assays we used a northern
470 blot probe to the 3' UTR and thus also detected the ZIKV sfRNA (Figure 3A and Figure 3B).
471 Overall a decrease in ZIKV gRNA coincided with a decrease in sfRNA, although the abundance
472 of sfRNA was greater than the gRNA, likely because both translating and newly-replicated ZIKV
473 RNA were degraded by Xrn1 (Figure 3B).
474
475 We next examined the effect of depleting SG proteins on viral titers by plaque assay (Figure 3C).
476 While, depletion of TIA-1 and TIAR had no effect on the production of infectious virus, depletion
477 of Ataxin-2, G3BP1 and YB1 significantly reduced viral titers. Consistent with the increase in ZIKV
478 protein and RNA following depletion of HuR, we also observed a significant increase in viral titers
479 (Figure 3C).
480
481 To ensure the effects on ZIKV following siRNA depletion of the SG proteins were not a result of
482 a change in cell viability, we quantified ATP levels in metabolically active cells from Huh7 cells
483 transfected with the respective siRNAs. The cell viability assay showed no significant differences
484 in the metabolic activity in cells depleted of Ataxin-2, G3BP1, HuR, TIA-1, TIAR and YB1,
485 indicating that the changes in ZIKV protein, RNA, and viral titers were the consequence of
486 knockdown of the specific SG protein (Figure 3D).
487
488 Because siRNA-depletion of G3BP1 and HuR showed the most dramatic effect on ZIKV gene
489 expression, we chose to focus on these two SG proteins in subsequent experiments. To confirm
490 the effect of G3BP1 and HuR on ZIKV gene expression, we overexpressed G3BP1-Flag and
491 HuR-Flag in ZIKV-infected cells and examined viral RNA levels and viral titers (Figure 3E and
492 Figure 3F). Analysis of viral RNA abundance showed that overexpression of G3BP1 and HuR
493 significantly increased and decreased ZIKV RNA, respectively (Figure 3E). Consistent with the
494 effects on ZIKV RNA, we observed a corresponding increase and decrease in viral titers following
495 overexpression of G3BP1 and HuR (Figure 3F). Together these data indicate TIA-1, TIAR and
496 YB1 regulate translation of the ZIKV polyprotein, and have a role in replication of the viral genome
497 (Figure 3A and Figure 3B). The significant decrease in viral titer following depletion of YB1 further
498 suggest a role for this cellular RNA-binding protein in virus assembly (Figure 3C). Ataxin-2 and

499 G3BP1 are proviral cellular factors as depletion of Ataxin-2 and G3BP1 decreased ZIKV RNA
500 levels (Figure 3A and 3B), and overexpression of G3BP1 increased viral RNA (Figure 3E), which
501 in turn affected the production of infectious particles (Figure 3F). Finally, HuR exhibits antiviral
502 activity as depletion of this RNA-binding protein significantly increased ZIKV protein and RNA
503 levels and viral titers, and overexpression of HuR-Flag showed a reciprocal effect on ZIKV gene
504 expression (Figure 3).
505
506 **Changing the abundance of G3BP1 and HuR affects ZIKV replication.** Depletion of G3BP1
507 and HuR significantly decreased and increased ZIKV gene expression respectively (Figure 3),
508 suggesting a role for these SG proteins in ZIKV translation and/or replication. To decipher the
509 function of G3BP1 and HuR in ZIKV gene expression, we used the replication-competent (WT)
510 and -deficient (Pol-) *Gaussia* luciferase (GLuc) ZIKV reporter plasmid (pCDNA6.2 MR766 clGLuc
511 Intron3127 HDVr, Figure 4A). These pCDNA6.2 MR766 clGLuc Intron3127 HDVr constructs were
512 derived from the cDNA clone containing the full-length genome of the Uganda MR766 strain under
513 the control of the cytomegalovirus (CMV) promoter (Figure 4A) (47). Specifically, the full-length
514 GLuc reporter gene, along with its signal sequence and the sequence for the foot-and-mouth
515 disease virus (FMDV) 2A peptide, was cloned as a translational fusion following the first 20 amino
516 acids of the capsid protein, and the full-length viral polyprotein was cloned downstream of GLuc.
517 To avoid aberrant genome cyclization during replication dues to duplicated 5' cyclization
518 elements, the flavivirus cyclization sequences in full length capsid coding region were disrupted
519 by silent mutagenesis. Following transfection of this reporter construct, transcription and 5'-end
520 capping of ZIKV genomic RNA are directed by the host, and the hepatitis D virus ribozyme (HDVr)
521 at the end of the 3' UTR cleaves the ZIKV genomic RNA to create an authentic 3' end (Figure 4A)
522 (47). Using GLuc expression as a proxy for viral RNA, translation of capped ZIKV RNA is detected
523 6 hours post-transfection. Translation of the ZIKV polyprotein, including the synthesis of NS5, the
524 RNA-dependent-RNA polymerase (RdRp), directs replication of the reporter genome such that
525 the increase in viral RNA as a result of replication is observed at 48- and 96-hours post-
526 transfection. We also expressed a ZIKV GLuc reporter genome that contained a mutation in the
527 RdRp active site (GDD-to-GNN; pCDNA6.2 MR766 clGLuc Intron3127 Pol(-) HDVr) which
528 rendered this mutant GLuc reporter genome replication-deficient (Pol-). Expression of the Pol(-)
529 reporter genome showed a clear difference between replicating WT genomes and ZIKV RNA
530 transcribed from the transfected plasmid at 48- and 96-hours post-transfection (Figures 4B-4E).
531

532 To elucidate effects on translation and replication we examined expression of the ZIKV GLuc
533 reporter genome following siRNA depletion or overexpression of G3BP1 and HuR (Figures 4B-
534 4E). RNAi depletion or overexpression of G3BP1 and HuR did not significantly affect GLuc
535 expression at 6- and 24-hours post-transfection of both the ZIKV WT and Pol(-) reporter genomes
536 (Figures 4B-4E), indicating that these two SG proteins do not affect translation of the ZIKV
537 genome (Figures 4B-4E). At 96 hours post-transfection of the WT reporter genome however,
538 siRNA depletion and overexpression of G3BP1 notably decreased and increased GLuc
539 expression respectively, showing that G3BP1 facilitates ZIKV replication (Figure 4B and Figure
540 4C). Curiously, overexpression of G3BP1 also increased GLuc expression from the ZIKV Pol(-)
541 reporter genome (Figure 4C). Since this ZIKV Pol(-) reporter genome is replication deficient, the
542 increased levels of host-transcribed ZIKV mRNA might be the result of G3BP1 binding (39) and
543 stabilizing the viral mRNA. In contrast to the effect of G3BP1, at 96 hours post-transfection
544 depletion of HuR dramatically increased GLuc expression (Figure 4D). Reciprocally,
545 overexpression of HuR decreased luciferase units compared to expression of the 3xFlag-BAP
546 control (Figure 4E), indicating that HuR negatively impacts the ZIKV replication. Taken together
547 these data support a role for G3BP1 and HuR in replication of the ZIKV genome.
548
549 **G3BP1 and HuR localize with ZIKV replication complexes.** To further demonstrate a role for
550 G3BP1 and HuR in ZIKV replication, we next examined the localization of these two SG proteins
551 at replication complexes (Figure 5). We first examined the localization of G3BP1 and HuR at
552 replication complexes by immunofluorescence analysis. In particular, we used antibodies to
553 dsRNA and ZIKV NS5 protein as markers for replication sites (Figure 5A and Figure 5B). While
554 dsRNA is a replication intermediate of negative-and positive-sense dsRNA, NS5 is critical for the
555 replication of the ZIKV RNA as it functions as the RdRp and the methyltransferase that caps the
556 5' end of the ZIKV genome (1). G3BP1 shows diffuse cytoplasmic staining in mock-infected cells,
557 however in ZIKV-infected cells we observed strong co-localization of G3BP1 with dsRNA (Figure
558 5A), and some co-localization with NS5 in the cytoplasm (Figure 5A). In mock-infected cells, HuR
559 was predominantly localized in the nucleus (Figure 5B). Consistent with the subcellular
560 fractionation data (Figure 2B and Figure 2C) we observed an increase in the localization of HuR
561 in the cytoplasm of ZIKV-infected cells (Figure 5B). Although HuR did not co-localize with dsRNA
562 in ZIKV-infected cells, we did note HuR staining adjacent to ZIKV replication sites (Figure 5B).
563 HuR showed similar localization with NS5 in the cytoplasm (Figure 5B). The localization of G3BP1
564 and HuR with respect to ZIKV replication sites support a role in the synthesis of viral RNA.

565

566 Similar to other immunofluorescence studies (49), we observed strong nuclear and weak
567 cytoplasmic localization for the ZIKV NS5 protein (Figure 5A and Figure 5B). Such localization
568 was consistent with the cytoplasmic/nuclear fractionation data (Figure 2B, Figure 2C and Figure
569 2D). Because both NS5 and HuR are largely nuclear, we anticipated that these proteins might co-
570 localize. Although immunofluorescence analysis showed diffuse nuclear staining for both NS5
571 and HuR, HuR did not co-localize with NS5 foci in the nucleus (Figure 5B). Both HuR and flavivirus
572 NS5 proteins have been shown to affect RNA splicing (51). While it is possible that HuR and NS5
573 together in the nucleus might modulate processing of cellular RNAs, further interaction studies
574 would need to be undertaken to verify such a role.

575

576 To corroborate the immunofluorescence analyses and role for G3BP1 and HuR in ZIKV
577 replication, we also isolated replication complexes from mock- and ZIKV-infected Huh7 cells by
578 sucrose gradient ultracentrifugation, and then investigated the localization of select SG proteins
579 with replication complexes. Western blot analysis showed the isolated fractions were derived from
580 the endoplasmic reticulum as shown by calnexin immunostaining in both mock and ZIKV-infected
581 fractions, and NS5 protein was only isolated in membrane fractions isolated from ZIKV-infected
582 cells. G3BP1 and HuR were isolated with the replication complexes (Figure 5C). TIA-1, TIAR and
583 YB1 have previously been shown to affect WNV replication (30, 36), we only observed a small
584 amount of TIA-1 and YB1 in the enriched membranes (Figure 5C). While we noted an increase in
585 the Ataxin-2 levels in ZIKV infected cells (Figure 2A), Ataxin-2 did not sediment with replication
586 complexes (Figure 5C). That G3BP1 and HuR were isolated with replication complexes (Figure
587 5C) further indicates that G3BP1 and HuR function to modulate ZIKV replication (Figure 4).

588

589 **G3BP1 co-localizes with ZIKV envelope protein.** Because ZIKV replication and assembly occur
590 in close proximity on cellular membranes, and G3BP1 was previously shown to interact with the
591 capsid protein (39), we also investigated whether G3BP1 and HuR co-localized with ZIKV
592 assembly sites. In particular, we examined the co-localization of both proteins with ZIKV envelope
593 (E) protein by immunofluorescence analysis (Figure 6). Similar to the localization of HuR with
594 dsRNA and ZIKV NS5 protein (Figure 5B) a small amount of HuR co-localized with ZIKV envelope
595 protein (Figure 6A). Interestingly, G3BP1 showed co-localization with the envelope protein in cells
596 infected with the Cambodia ZIKV strain (Figure 6A) and with the Puerto Rican (PRVABC59) and
597 Ugandan (MR766) strains of ZIKV (Figure 6B). The co-localization of G3BP1 with the ZIKV

envelope protein together with the siRNA studies showing that depletion of G3BP1 modestly decreased ZIKV RNA by ~40% (Figure 3B), while viral titers were dramatically reduced (Figure 3C), raise the possibility that G3BP1 might function more broadly than previously recognized. Specifically, G3BP1 promotes replication of the ZIKV genome and maybe also the assembly of new viral particles.

Discussion:

The formation and sequestration of components of the translation machinery in SGs function as an intrinsic antiviral mechanism to restrict viral translation and/or replication. Flaviviruses have been shown to limit stress granule assembly by affecting cellular pathways. Specifically WNV was shown to modulate the cellular redox response by increasing the levels of the transcription factors that activate antioxidant genes and increase reduced glutathione levels (32). DENV modulates stress granule assembly by changing the phosphorylation of the cap-binding protein eIF4E by altering p38-Mnk1 signaling to affect cellular translation (33). More recently, ZIKV was shown to increase the rate of eIF2α dephosphorylation which would promote translation and the rapid disassembly of stress granules (40). Interestingly, Hou *et al.*, also showed that specific viral proteins impact cellular translation and the formation of stress granules (39). We similarly observed fewer SGs in ZIKV-infected cells, and that the assembly of SGs following sodium arsenite-treatment was inhibited during ZIKV infection (Figure 1). Proceeding depletion of TIAR, G3BP1 and Caprin-1, Hou *et al.*, also found decreased ZIKV viral titers (39). In our study we present a systematic investigation of the role of six different SG proteins on ZIKV protein and RNA abundance, production of infectious particles, the co-localization with ZIKV and effects on replication. Although G3BP1 from A549-infected cells co-immunopreciptated ZIKV RNA (39), we specifically show that G3BP1 is in replication complexes (Figure 5) and promotes synthesis of ZIKV RNA (Figure 4B and Figure 4C). Hou *et al.*, also demonstrated that G3BP1 interacted with overexpressed Flag-tagged ZIKV capsid protein (39). We found that in ZIKV-infected cells G3BP1 co-localized with ZIKV envelope protein which raises the possibility that G3BP1 may facilitate virion assembly in addition to its role in ZIKV replication (Figure 6). Excitingly, we show that HuR functions to limit ZIKV replication, which to our knowledge has not previously been shown for this cellular RNA binding protein. Our systematic analysis of SG proteins during ZIKV infection is significant particularly as G3BP1, HuR and other SG proteins have an intimate role in neurodevelopment and function. The modulation of SGs and SG proteins by ZIKV may have a more significant impact on normal gene regulation that contributes to ZIKV pathogenesis.

631

632 Ataxin-2 is a cytosolic SG protein that is associated with the neurodegenerative disorder
633 spinocerebellar ataxia type-2 (SCA2) (52, 53). During ZIKV infection we observed an increase in
634 the abundance of Ataxin-2 (Figure 2A). Furthermore, RNAi studies showed that depletion of
635 Ataxin-2 did not affect ZIKV capsid levels (Figure 3A) but did decrease the amount of viral RNA
636 and viral titers (Figure 3B and Figure 3C). Ataxin-2 levels have been shown to affect the
637 abundance of the poly(A) binding protein (PABP) (53), where elevated levels of Ataxin-2
638 decreased the amount of PABP (53). Such changes in PABP would be expected to negatively
639 affect translation of cellular mRNAs and promote ZIKV gene expression. Moreover, Ataxin-2
640 interacts with the cellular RNA DEAD-box helicase DDX6 (53), which we have previously shown
641 to be required for ZIKV gene expression (54). Therefore, the impact on ZIKV RNA and production
642 of infectious particles (Figure 3B and Figure 3C) following RNAi depletion of Ataxin-2 might also
643 be the result of changes to DDX6. Analysis of SCA2 brains showed an increase in Ataxin-2 levels
644 and that Ataxin-2 localized in intranuclear inclusions in 1-2% of neurons (55, 56). Our data
645 showing that Ataxin-2 modulates ZIKV gene expression in the hepatocellular carcinoma cell line
646 Huh7 is exciting and additional studies in neuronal cells would illuminate the role of this protein in
647 cellular dysfunction and neurodegeneration following intrauterine ZIKV infection.

648

649 The RNA-binding proteins TIA-1 and TIAR are broadly expressed in cells and tissues (57). These
650 proteins are predominantly localized in the nucleus (Figure 1, and data not shown), have been
651 shown to modulate translation of specific cellular mRNAs (58) and are critical nucleators of stress
652 granules in the cytoplasm (27). During WNV and DENV infection TIA-1 and TIAR co-localize at
653 replication sites, and bind to the 3' stem loop region in the negative-strand of WNV RNA to
654 promote replication (30, 36, 59). We determined by western blot analysis that TIA-1, but not TIAR,
655 localized in isolated replication complexes (Figure 5C). Because TIA-1 and TIAR were previously
656 shown to promote WNV replication we also investigated the role of TIA-1 and TIAR during ZIKV
657 infection. Similar to Hou *et al.* (39), we found that decreasing the levels of TIA-1 had no effect on
658 viral titers (Figure 3C). In contrast to Hou *et al.* (39), we found that that depletion of TIAR did not
659 affect ZIKV titers (Figure 3C). Our RNAi studies also demonstrated that following the reduction of
660 TIA-1 and TIAR levels, the abundance of ZIKV capsid protein increased (Figure 3A), and
661 depletion of TIAR decreased ZIKV RNA levels (Figure 3A and Figure 3B), suggesting that, similar
662 to tick-borne encephalitis virus, TIA-1 and TIAR are re-localized to perinuclear regions of
663 replication to modulate translation of the ZIKV polyprotein (60). While the role of TIA-1 and TIAR

664 in our studies in Huh7 differs from the study by Hou and colleagues which were undertaken in
665 A549 cells (39), the impact of TIA-1 and TIAR might be better elucidated in neuronal cells where
666 a link between TIA-1, the microtubule protein Tau and the neurodegenerative tauopathies has
667 been described (61, 62).
668
669 Y box-binding protein-1 (YB1) modulates translation and stabilizes cellular mRNAs (58) and also
670 localizes in processing bodies and stress granules (63). YB1 has been shown to bind the DENV
671 3' UTR to decrease DENV translation (64). In our study, siRNA depletion of YB1 increased the
672 levels of ZIKV capsid protein (Figure 3A) indicating that YB1, similar to the role in DENV infection,
673 negatively regulates ZIKV translation. We also observed that YB1 is localized in replication
674 complexes (Figure 5C) and that depleting YB1 levels decreases ZIKV RNA levels (Figure 3B).
675 Notably however, the modest effects of YB1 reduction on ZIKV protein and RNA levels differ from
676 the significantly decreased viral titers (Figure 3C). YB1 was previously shown to interact with the
677 hepatitis C virus NS3/4A protein, and other cellular factors, to modulate the balance between
678 replication and the assembly of HCV infectious particles (65, 66), and additional studies with YB1
679 may reveal a similar function during ZIKV infection.
680
681 G3BP1, similar to TIA-1, is an important nucleator of SGs (26, 28, 67). Interestingly, the role of
682 G3BP1 varies in viral infections from limiting alphavirus replication (68–70) to interacting with the
683 HCV RdRp NS5B and enhancing the production of HCV infectious virus particles (43, 71, 72). In
684 DENV-infected cells, G3BP1 interacts with the sfRNA (37, 73), and sequestration of G3BP1 by
685 the sfRNA was shown to inhibit translation of interferon-stimulated genes (38). Hou *et al.*, showed
686 that siRNA depletion of G3BP1 decreased ZIKV titers and that G3BP1 also bound ZIKV RNA
687 (39). In addition to the dramatic reduction in ZIKV titers following depletion of G3BP1 (Figure 3C)
688 we also observed a decrease ZIKV protein and RNA levels (Figure 3A and Figure 3B). Together
689 these data suggested a role for G3BP1 in ZIKV translation, replication, and/or assembly. In our
690 study we also used the ZIKV MR766 GLuc reporter genome (Figure 4B and Figure 4C) and
691 showed a specific role in ZIKV replication, which was further supported by the localization of
692 G3BP1 with ZIKV replication complexes (Figure 5C) and co-localized with dsRNA (Figure 5A).
693 We also observed that ZIKV envelope protein (Figure 6) co-localized with G3BP1 suggesting that
694 in addition to facilitating replication of the ZIKV genome, G3BP1 may have a role in assembly of
695 new virus particles. Hou and colleagues report that G3BP1 binds ZIKV gRNA and that G3BP1
696 and Caprin-1 interact with the ZIKV capsid protein to increase ZIKV gene expression. While

697 further mechanistic studies are required to demonstrate a role for G3BP1 in ZIKV assembly, it is
698 possible that a multi-protein complex between ZIKV RNA, capsid protein, G3BP1 and Caprin-1
699 may shift the equilibrium from replication of the viral genome towards localization with the ZIKV
700 envelope protein and the assembly of infectious ZIKV particles.
701
702 Human antigen R (HuR) is a member of the ELAVL RNA-binding protein family and is ubiquitously
703 expressed (74). Notably, the three additional members of the ELAVL family (HuB/C/D) are highly
704 expressed in the brain (74). HuR binding to poly-U and AU-rich elements within the 3' UTR
705 increases mRNA stability (75, 76). During infection with the single-stranded positive-sense
706 alphaviruses Sindbis virus (SINV) and Chikungunya virus (CHIKV), HuR was dramatically re-
707 localized from the nucleus into the cytoplasm (77, 78). By subcellular fractionation and western
708 blot analysis we similarly observed that HuR is re-distributed into the cytoplasm (Figure 2B), albeit
709 not to the same extent as during alphavirus infection (77, 78). HuR is recruited to alphavirus RNA
710 via the U-rich elements within the 3' UTR and this interaction stabilizes and protects the viral RNA
711 from the cellular mRNA decay machinery (78). Although HuR has been shown to promote
712 alphavirus mRNA stability (77, 78) and HCV IRES-mediated translation (43, 79) our study
713 indicates an antiviral role for HuR during ZIKV infection (Figure 3), which to our knowledge has
714 not previously been shown. In particular we found that HuR modulates ZIKV replication (Figure
715 4D and Figure 4E) which resulted in increased ZIKV protein and RNA levels and viral titers (Figure
716 3). The role of HuR in ZIKV replication was further supported by the detection of HuR in isolated
717 replication complexes (Figure 5C). Curiously, immunofluorescence studies showed that HuR in
718 the cytoplasm was localized adjacent to dsRNA and ZIKV NS5 protein staining (Figure 5B). We
719 note that the localization of HuR in replication complexes when analyzed in isolated replication
720 complexes versus immunofluorescence analysis do not strongly correlate. However, it is
721 important to highlight that HuR is strongly localized in the nucleus (Figure 5B and 6A) and this
722 nuclear staining likely overshadows the re-localization of HuR into the cytoplasm and replication
723 complexes. Indeed, immunofluorescence analysis of ZIKV NS5 protein similarly showed strong
724 nuclear and weak cytoplasmic localization (Figure 5B), despite being the RdRp responsible for
725 replicating the ZIKV RNA genome. A role for HuR in ZIKV replication was further supported by
726 siRNA depletion of HuR and overexpression of HuR-Flag that increased and decreased
727 replication of the MR766 GLuc reporter expression respectively (Figure 4D and Figure 4E). The
728 mode by which HuR limits ZIKV replication remains to be elucidated. A bioinformatic analysis of
729 the ZIKV 3' UTRs identified putative HuR binding sites (data not shown), raising the possibility

730 that similar to SINV (78), HuR interacts with ZIKV RNA to alter the subcellular localization of HuR,
731 and directly affect ZIKV replication, possibly by destabilizing, rather than stabilizing, the viral RNA.
732 Alternatively, the consequence on ZIKV replication might be indirect where HuR re-localization
733 affects cellular RNA homeostasis or ribostasis. Indeed, re-localization of HuR by SINV into the
734 cytoplasm was shown to decrease cellular mRNA stability and alter mRNA splicing and nuclear
735 polyadenylation (80). Interestingly, another cell RNA-binding protein Fragile X mental retardation
736 factor (FMRP) was shown to bind ZIKV sfRNA and limit viral infection (81). It will be interesting to
737 determine the mechanism by which HuR functions during ZIKV, and whether this regulatory mode
738 is similar to FMRP. Such studies will provide new insights into viral-host interactions, particularly
739 for RNA-binding proteins that function as restriction factors.
740
741 Beyond aggregating stalled translation complexes, RNA binding proteins in stress granules also
742 localize in neuronal granules. These granules regulate neuronal growth and synaptic plasticity
743 (82, 83). Interestingly, a number of stress granule proteins such as Ataxin-2, G3BP1, TIA-1 and
744 HuR are known to contribute to different neuropathologies (41, 83). While transcriptional changes
745 have been reported to contribute to the neurological and developmental defects observed
746 following intrauterine ZIKV-infection (84–87), the role of stress granules and granule proteins
747 should not be overlooked. By limiting the formation of stress granules, and re-localizing and
748 subverting specific stress granule proteins, alterations in RNA homeostasis, such as changes in
749 RNA splicing, RNA stability and translation, could also contribute to ZIKV neuropathologies. To
750 this end, elucidating the interactions of stress granule proteins and the cellular consequences
751 particularly in neuronal cells could provide new insights into the pathomechanisms underlying
752 ZIKV congenital disease.
753
754 **Acknowledgements:**
755 We thank Dr. Brett Lindenbach (Yale School of Medicine) for ZIKV Cambodian-isolate (160310)
756 and Ugandan-isolate (MR766), and Dr. Laura Kramer (Wadsworth Center, NYSDOH) and the
757 CDC for the Puerto Rican-isolate (PRVABC59). We also thank members of the Pager lab,
758 Marlene Belfort, Gabriele Fuchs and Ing-Nang Wang for valuable comments and suggestions on
759 the manuscript.
760
761
762

Funding:

This work was supported by start-up funds from University at Albany-SUNY and New York State, the University at Albany Presidential Initiatives Fund for Research and Scholarship (PIFRS) to CTP; and NIH grants (R21 AI133617-01 and R01 GM123050) to CTP. MJE received funding from the Burroughs Wellcome Fund Investigators in Pathogenesis of Infectious Disease Award and NIH grants (R21 AI133649 and R21 AI140196).

770 **Figure Legends:**

771

772 **Figure 1. ZIKV restricts the assembly of cellular stress granules.** Huh7 cells were either
773 mock-infected or infected with the Cambodia ZIKV-strain (160310) at a MOI of 5. Twenty-four
774 hours post-infection cells were mock-treated or incubated with 1 mM sodium arsenite for 30
775 minutes, fixed, permeabilized, and analyzed using a 63x oil immersion objective on a Zeiss
776 LSM710 laser scanning confocal microscope. ZIKV-infected cells were detected with mouse-anti-
777 dsRNA antibody (green). The distribution of dsRNA (green) and the stress granule (SG) marker
778 TIA-1 (red) in mock- and ZIKV-infected cells A) not treated and B) treated with sodium arsenite.
779 The white arrows highlight stress granules. Quantification of SGs containing Ataxin-2, G3BP1,
780 eIF3B, HuR, TIA-1, TIAR and YB1 proteins in mock- and ZIKV (Cambodia-160310)-infected which
781 were either C) not treated or D) treated with sodium arsenite. The number of cells containing
782 G3BP1, eIF3, and TIA-1-containing SGs in mock-infected cells or cells infected with a Puerto
783 Rican isolate of ZIKV at a MOI of 5 and either E) not treated or F) treated with sodium arsenite.
784 G-H) SGs in mock-infected cells and cells infected with the original Ugandan isolate of ZIKV at a
785 MOI of 5 were quantified. The number of cells containing G3BP1, eIF3, and TIA-1-SG was
786 quantified from cells that were G) untreated or H) incubated with sodium arsenite. Note, in the
787 original immunofluorescence images, TIA-1 was visualized using an anti-donkey Alexa Fluor®
788 647 (magenta) anti-goat IgG secondary antibody. In panels A) and B) TIA-1 has been pseudo-
789 colored red. The immunofluorescence images are representative of at least three independent
790 experiments. The errors bars shown on the SG quantification data (Panel 1C, 1D, 1E, 1F, 1G,
791 and 1H) are of the mean ± SD. Significance was determined by two-tailed student T-test (*$P<0.05$;
792 **$P<0.01$; ***$P<0.001$; and N.S. not significant).

793

794 **Figure 2. ZIKV infection changes the nuclear and cytoplasmic distribution of stress granule**
795 **proteins.** A) Huh7 cells infected with the Cambodia strain of ZIKV at MOI of 1 or 5 were harvested
796 at 1, 2, and 3 days post-infection. Detection of ZIKV capsid protein by western blot confirmed viral
797 infection. The abundance and integrity of Ataxin-2, G3BP1, HuR, TIA-1 and TIAR proteins was
798 also examined at each time point. The western blot shown is representative of at least three
799 independent experiments. B) Western blot analysis of SG proteins in MR766 and PRVABC59-
800 infected Huh7 cells 3 days post-infection. C) Cytoplasmic and nuclear distribution of Ataxin-2,
801 G3BP1, HuR, TIA-1, TIAR and YB1. Huh7 cells were mock-infected or infected with the Cambodia
802 strain of ZIKV at MOI of 5 and 1-day post-infection the cytoplasmic and nuclear fractions were

803 isolated. The distribution of ZIKV NS5, Ataxin-2, G3BP1, HuR, TIA-1, TIAR, YB1, GRP78 and
804 Fibrillarin was analyzed by western blot. The western blot shown is representative of the three
805 independent experiments performed. Quantification of the distribution of Ataxin-2, G3BP1, HuR,
806 TIA-1, TIAR and YB1 in the D) cytoplasmic and E) nuclear subcellular fractions. The abundance
807 of each SG protein in the cytoplasmic or nuclear fraction was standardized against GRP78 or
808 Fibrillarin, respectively. These values were then normalized against the abundance of the specific
809 SG protein in mock-infected cells, which was assigned the arbitrary unit (a.u.) of one (denoted by
810 dashed line on each graph). The data presented in panels D) and E) were calculated from three
811 independent infections, fractionations and immunoblots. F) Quantification of fluorescence
812 intensity signal of the localization of HuR in the nucleus. Fluorescence intensity was derived in
813 ImageJ using a freehand selection of the nucleus in mock- and ZIKV-infected cells. Values
814 obtained for HuR were divided by the nucleus signal (Hoechst) within mock- and ZIKV-infected
815 cells. Fluorescence intensity of the infected cells were standardized against mock-infected cells
816 and arbitrarily assigned a value of 1. The relative fluorescence intensity signal was calculated
817 from three independent experiments and nine cells were counted per experiment. Two-tailed
818 student T-tests were performed to calculate significance with *P<0.05, ***P<0.001, and N.S. not
819 significant.
820
821 **Figure 3. Stress granule proteins promote and limit ZIKV gene expression.** Ataxin-2, G3BP1,
822 HuR, TIA-1, TIAR and YB1 proteins were depleted in Huh7 cells using target-specific siRNAs,
823 and then infected 24 hours later at a MOI of 5 with the Cambodia strain of ZIKV (160310). A
824 siRNA targeting *Gaussia* luciferase (siGL2) was used as a control, non-targeting siRNA. Protein,
825 RNA and media were harvested 48 hours post-infection. A) Western blot shows expression of
826 ZIKV capsid, and depletion of each stress granule protein. Expression of GAPDH was used as a
827 loading control, and the western blot shown is representative of at least three independent
828 experiments. The northern blot shows the effect of depleting each stress granule protein on the
829 abundance of the ZIKV genomic (gZIKV) and subgenomic flaviviral (sfZIKV) RNA. Actin mRNA
830 levels were evaluated as a loading control. The northern blot shown is representative of at least
831 three independent experiments. B) Quantification of ZIKV gRNA and sfRNA. ZIKV RNA levels
832 were normalized to actin mRNA, and then represented relative to siGL2 control. C) Viral titers in
833 the extracellular media were determined by plaque assay and relative viral titers were calculated
834 by normalizing titers relative to siGL2 transfected cells. D) A representative assay showing the
835 effect of siRNA depletion of the six SG proteins on cell viability. E) Quantification of ZIKV RNA

836 levels following overexpression of G3BP1-Flag and HuR-Flag. Huh7 cells were transfected with
837 plasmids expressing 3xFlag-Bacterial Alkaline Phosphatase (BAP; control), G3BP1-Flag or HuR-
838 Flag, and then infected with ZIKV (Cambodia-160310) 24 hours post-infection. The effect of
839 overexpressing G3BP1-Flag and HuR-Flag on gZIKV and sfZIKV RNA was evaluated by northern
840 blot. F) Effect of overexpression of G3BP1-Flag and HuR-Flag on viral titers. Data presented in
841 Figure 3 are from at least three independent experiments. Error bars show mean ± SD, and
842 statistical significance was determined using a two-tailed student T-test (*P<0.05; **P<0.01;
843 ***P<0.001; N.S. not significant).
844
845 **Figure 4. G3BP1 and HuR modulate ZIKV replication.** A) Schematic of the ZIKV MR766
846 *Gaussia* luciferase reporter genome within the pCDNA6.2 MR766 clGLuc Intron3127 HDVr
847 plasmid showing the 5' and 3' UTRs, the mature viral proteins within the single-open reading
848 frame, as well as the position of the *Gaussia* luciferase gene within the MR766 genome. Two
849 elements within the plasmid namely the CMV promoter and the HDVr, which creates an authentic
850 3' UTR in the genome, are also denoted. B & D) Huh7 cells were first transfected with either the
851 control or target-specific siRNAs, and then transfected with the same siRNAs and the pCDNA6.2
852 MR766 clGLuc Intron3127 HDVr WT replication-competent or Pol(-) replication-deficient
853 plasmids. GLuc activity in the media of transfected cells was assayed at 6, 24, 48, and 96 hours
854 post-transfection. C & E) Huh7 cells were transfected with p3xFlag-BAP, pG3BP1-Flag, pHuR-
855 Flag and WT and Pol(-) pCDNA6.2 MR766 clGLuc Intron3127 HDVr. At 6, 24, 48, and 96 hours
856 post-transfection media from the transfected cells was collected and GLuc activity measured. B)
857 Effect of G3BP1 knockdown on ZIKV-GLuc genome expression. C) Effect on ZIKV-GLuc reporter
858 genome expression following overexpression of 3xFlag-BAP (control) and G3BP1-Flag. D) Effect
859 of depleting HuR on ZIKV-GLuc genome expression. E) Effect of overexpressing 3xFlag-BAP and
860 HuR-Flag on ZIKV-GLuc genome expression. The data shown in Figure 4B-4E are from a single
861 experiment and are representative of at least three independent experiments. Error bars indicate
862 mean ± SD.
863
864 **Figure 5. G3BP1 and HuR localize with ZIKV replication complexes.** A-B) Huh7 cells were
865 either mock-infected or infected with the Cambodia ZIKV strain at a MOI of 5. One day post-
866 infection cells were fixed, permeabilized, and prepared for confocal imaging. Immunofluorescence
867 images are representative of at least three independent experiments. A) Immunofluorescence
868 image showing G3BP1 (red) localization in mock- infected cells and with viral replication sites as

869 visualized by the staining with antibodies to dsRNA and NS5 (green) in ZIKV-infected cells. B)
870 Localization of HuR (red) in mock-infected cells and with dsRNA and NS5 (green) in ZIKV-infected
871 cells. C) Western blot analysis of ZIKV NS5, Ataxin-2, G3BP1, HuR, TIA-1, TIAR, YB1, and
872 calnexin associated with replication complexes isolated from mock- and ZIKV-infected Huh7 cells.
873 The western blot is representative of three independent experiments.
874
875 **Figure 6. G3BP1 co-localizes with ZIKV E protein.** One day post-infection Huh7 cells infected
876 with ZIKV at a MOI of 5 were fixed, permeabilized, and prepared for confocal imaging. A)
877 Localization of ZIKV E protein with HuR and G3BP1 following infection with the Cambodia strain
878 of ZIKV. B) Localization of ZIKV E protein with G3BP1 following infection with the Puerto Rican
879 (PRVABC59) and Ugandan (MR766) strains of ZIKV, respectively. The immunofluorescence
880 images shown are representative of at least three independent experiments.
881

882 **References:**

883 1. Lindenbach BD, Murray CL, Thiel H-J, Rice CM. 2013. FlaviviridaeFields Virology, 6th ed.
884 Lippincott Williams & Wilkins, Philadelphia, PA.

885 2. Dick GWA. 1952. Zika Virus (I). Isolations and serological specificity. Trans R Soc Trop
886 Med Hyg 46:509–520.

887 3. Faria NR, Azevedo R do S da S, Kraemer MUG, Souza R, Cunha MS, Hill SC, Thézé J,
888 Bonsall MB, Bowden TA, Rissanen I, Rocco IM, Nogueira JS, Maeda AY, Vasami FG da
889 S, Macedo FL de L, Suzuki A, Rodrigues SG, Cruz ACR, Nunes BT, Medeiros DB de A,
890 Rodrigues DSG, Queiroz ALN, da Silva EVP, Henriques DF, da Rosa EST, de Oliveira
891 CS, Martins LC, Vasconcelos HB, Casseb LMN, Simith D de B, Messina JP, Abade L,
892 Lourenço J, Alcantara LCJ, de Lima MM, Giovanetti M, Hay SI, de Oliveira RS, Lemos P
893 da S, de Oliveira LF, de Lima CPS, da Silva SP, de Vasconcelos JM, Franco L, Cardoso
894 JF, Vianez-Júnior JL da SG, Mir D, Bello G, Delatorre E, Khan K, Creatore M, Coelho
895 GE, de Oliveira WK, Tesh R, Pybus OG, Nunes MRT, Vasconcelos PFC. 2016. Zika virus
896 in the Americas: Early epidemiological and genetic findings. Science (80-) 352:345–349.

897 4. Melo AS de O, Aguiar RS, Amorim MMR, Arruda MB, Melo F de O, Ribeiro STC, Batista
898 AGM, Ferreira T, dos Santos MP, Sampaio VV, Moura SRM, Rabello LP, Gonzaga CE,
899 Malinger G, Ximenes R, de Oliveira-Szejnfeld PS, Tovar-Moll F, Chimelli L, Silveira PP,
900 Delvechio R, Higa L, Campanati L, Nogueira RMR, Filippis AMB, Szejnfeld J, Voloch CM,
901 Ferreira OC, Brindeiro RM, Tanuri A. 2016. Congenital Zika Virus Infection. JAMA Neurol
902 73:1407–1416.

903 5. Martines RB, Bhatnagar J, de Oliveira Ramos AM, Davi HPF, Iglezias SDA, Kanamura
904 CT, Keating MK, Hale G, Silva-Flannery L, Muehlenbachs A, Ritter J, Gary J, Rollin D,
905 Goldsmith CS, Reagan-Steiner S, Ermias Y, Suzuki T, Luz KG, de Oliveira WK, Lanciotti
906 R, Lambert A, Shieh WJ, Zaki SR. 2016. Pathology of congenital Zika syndrome in Brazil:
907 a case series. Lancet 388:898–904.

908 6. Miner JJ, Diamond MS. 2017. Zika Virus Pathogenesis and Tissue Tropism. Cell Host
909 Microbe 21:134–142.

910 7. Russo FB, Jungmann P, Beltrão-Braga PCB. 2017. Zika infection and the development of
911 neurological defects. Cell Microbiol 19:e12744.

912 8. Coyne CB, Lazear HM. 2016. Zika virus — reigniting the TORCH. Nat Rev Microbiol
913 14:707–715.

914 9. Chan JFW, Choi GKY, Yip CCY, Cheng VCC, Yuen KY. 2016. Zika fever and congenital
915 Zika syndrome: An unexpected emerging arboviral disease. J Infect 72:507–524.

916 10. Cao-Lormeau V-M, Blake A, Mons S, Lastère S, Roche C, Vanhomwegen J, Dub T,
917 Baudouin L, Teissier A, Larre P, Vial A-L, Decam C, Choumet V, Halstead SK, Willison
918 HJ, Musset L, Manuguerra J-C, Despres P, Fournier E, Mallet H-P, Musso D, Fontanet A,
919 Neil J, Ghawché F. 2016. Guillain-Barré Syndrome outbreak associated with Zika virus
920 infection in French Polynesia: a case-control study. Lancet 387:1531–1539.

921 11. da Silva IRF, Frontera JA, Bispo de Filippis AM, Nascimento OJM do, RIO-GBS-ZIKV
922 Research Group. 2017. Neurologic Complications Associated With the Zika Virus in
923 Brazilian Adults. JAMA Neurol 74:1190–1198.

924 12. Parra B, Lizarazo J, Jiménez-Arango JA, Zea-Vera AF, González-Manrique G, Vargas J,

925 Angarita JA, Zuñiga G, Lopez-Gonzalez R, Beltran CL, Rizcala KH, Morales MT,
926 Pacheco O, Ospina ML, Kumar A, Cornblath DR, Muñoz LS, Osorio L, Barreras P, Pardo
927 CA. 2016. Guillain–Barré Syndrome Associated with Zika Virus Infection in Colombia. N
928 Engl J Med 375:1513–1523.

929 13. Oehler E, Watrin L, Larre P, Leparc-Goffart I, Lastere S, Valour F, Baudouin L, Mallet H,
930 Musso D, Ghawche F. 2014. Zika virus infection complicated by Guillain-Barre syndrome-
931 -case report, French Polynesia, December 2013. Euro Surveill 19:pii=20720.

932 14. Musso D, Roche C, Robin E, Nhan T, Teissier A, Cao-Lormeau VM. 2015. Potential
933 sexual transmission of zika virus. Emerg Infect Dis 21:359–361.

934 15. Besnard M, Lastere S, Teissier A, Cao-Lormeau VM, Musso D, Lastère S, Teissier A,
935 Cao-Lormeau VM, Musso D. 2014. Evidence of perinatal transmission of zika virus,
936 French Polynesia, December 2013 and February 2014. Eurosurveillance 19:pii=20751.

937 16. D'Ortenzio E, Matheron S, de Lamballerie X, Hubert B, Piorkowski G, Maquart M,
938 Descamps D, Damond F, Yazdanpanah Y, Leparc-Goffart I. 2016. Evidence of Sexual
939 Transmission of Zika Virus. N Engl J Med 374:2195–2198.

940 17. Mansuy JM, Dutertre M, Mengelle C, Fourcade C, Marchou B, Delobel P, Izopet J,
941 Martin-Blondel G. 2016. Zika virus: High infectious viral load in semen, a new sexually
942 transmitted pathogen? Lancet Infect Dis.

943 18. Edgil D, Polacek C, Harris E. 2006. Dengue virus utilizes a novel strategy for translation
944 initiation when cap-dependent translation is inhibited. J Virol 80:2976–2986.

945 19. Levin DH, Petryshyn R, London IM. 1980. Characterization of double-stranded-RNA-
946 activated kinase that phosphorylates subunit of eukaryotic initiation factor 2 (eIF-2) in
947 reticulocyte lysates. Proc Natl Acad Sci 77:832–836.

948 20. Harding HP, Zhang Y, Ron D. 1999. Protein translation and folding are coupled by an
949 endoplasmic-reticulum-resident kinase. Nature 397:271–274.

950 21. Dever TE, Feng L, Wek RC, Cigan AM, Donahue TF, Hinnebusch AG. 1992.
951 Phosphorylation of initiation factor 2α by protein kinase GCN2 mediates gene-specific
952 translational control of GCN4 in yeast. Cell 68:585–596.

953 22. Chen JJ, Throop MS, Gehrke L, Kuo I, Pal JK, Brodsky M, London IM. 1991. Cloning of
954 the cDNA of the heme-regulated eukaryotic initiation factor 2 alpha (eIF-2 alpha) kinase
955 of rabbit reticulocytes: homology to yeast GCN2 protein kinase and human double-
956 stranded-RNA-dependent eIF-2 alpha kinase. Proc Natl Acad Sci 88:7729–7733.

957 23. Protter DSW, Parker R. 2016. Principles and Properties of Stress Granules. Trends Cell
958 Biol 26:668–679.

959 24. Markmiller S, Soltanieh S, Server KL, Mak R, Jin W, Fang MY, Luo EC, Krach F, Yang D,
960 Sen A, Fulzele A, Wozniak JM, Gonzalez DJ, Kankel MW, Gao FB, Bennett EJ, Lécuyer
961 E, Yeo GW. 2018. Context-Dependent and Disease-Specific Diversity in Protein
962 Interactions within Stress Granules. Cell 172:590–604.e13.

963 25. Jain S, Wheeler JRR, Walters RWW, Agrawal A, Barsic A, Parker R. 2016. ATPase-
964 Modulated Stress Granules Contain a Diverse Proteome and Substructure. Cell 164:487–
965 498.

966 26. Tourrière H, Chebli K, Zekri L, Courselaud B, Blanchard JM, Bertrand E, Tazi J. 2003.

967 The RasGAP-associated endoribonuclease G3BP assembles stress granules. J Cell Biol
968 160:823–831.

969 27. Gilks N, Kedersha N, Ayodele M, Shen L, Stoecklin G, Dember LM, Anderson P. 2004.
970 Stress Granule Assembly Is Mediated by Prion-like Aggregation of TIA-1. Mol Biol Cell
971 15:5383–5398.

972 28. Kedersha N, Panas MD, Achorn CA, Lyons S, Tisdale S, Hickman T, Thomas M,
973 Lieberman J, McInerney GM, Ivanov P, Anderson P. 2016. G3BP-Caprin1-USP10
974 complexes mediate stress granule condensation and associate with 40S subunits. J Cell
975 Biol 212:845–860.

976 29. Tsai W-C, Gayatri S, Reineke LC, Sbardella G, Bedford MT, Lloyd RE. 2016. Arginine
977 Demethylation of G3BP1 Promotes Stress Granule Assembly. J Biol Chem 291:22671–
978 22685.

979 30. Emara MM, Brinton MA. 2007. Interaction of TIA-1/TIAR with West Nile and dengue virus
980 products in infected cells interferes with stress granule formation and processing body
981 assembly. Proc Natl Acad Sci 104:9041–9046.

982 31. Katoh H, Okamoto T, Fukuhara T, Kambara H, Morita E, Mori Y, Kamitani W, Matsuura
983 Y. 2013. Japanese Encephalitis Virus Core Protein Inhibits Stress Granule Formation
984 through an Interaction with Caprin-1 and Facilitates Viral Propagation. J Virol 87:489–
985 502.

986 32. Basu M, Courtney SC, Brinton MA. 2017. Arsenite-induced stress granule formation is
987 inhibited by elevated levels of reduced glutathione in West Nile virus-infected cells. PLoS
988 Pathog 13:e1006240.

989 33. Roth H, Magg V, Uch F, Mutz P, Klein P, Haneke K, Lohmann V, Bartenschlager R,
990 Fackler OT, Locker N, Stoecklin G, Ruggieri A. 2017. Flavivirus infection uncouples
991 translation suppression from cellular stress responses. MBio 8:e02150-16.

992 34. Elbahesh H, Scherbik SV, Brinton MA. 2011. West Nile virus infection does not induce
993 PKR activation in rodent cells. Virology 421:51–60.

994 35. Courtney SC, Scherbik S V., Stockman BM, Brinton M a. 2012. West Nile Virus Infections
995 Suppress Early Viral RNA Synthesis and Avoid Inducing the Cell Stress Granule
996 Response. J Virol 86:3647–3657.

997 36. Li W, Li Y, Kedersha N, Anderson P, Emara M, Swiderek KM, Moreno GT, Brinton MA.
998 2002. Cell proteins TIA-1 and TIAR interact with the 3' stem-loop of the West Nile virus
999 complementary minus-strand RNA and facilitate virus replication. J Virol 76:11989–2000.

1000 37. Ward AM, Bidet K, Yinglin A, Ler SG, Hogue K, Blackstock W, Gunaratne J, Garcia-
1001 Blanco MA. 2011. Quantitative mass spectrometry of DENV-2 RNA-interacting proteins
1002 reveals that the DEAD-box RNA helicase DDX6 binds the DB1 and DB2 3' UTR
1003 structures. RNA Biol 8:1173–86.

1004 38. Bidet K, Dadlani D, Garcia-Blanco MA. 2014. G3BP1, G3BP2 and CAPRIN1 Are
1005 Required for Translation of Interferon Stimulated mRNAs and Are Targeted by a Dengue
1006 Virus Non-coding RNA. PLoS Pathog 10:e1004242.

1007 39. Hou S, Kumar A, Xu Z, Airo AM, Stryapunina I, Wong CP, Branton W, Tchesnokov E,
1008 Götte M, Power C, Hobman TC. 2017. Zika Virus Hijacks Stress Granule Proteins and
1009 Modulates the Host Stress Response. J Virol 91:e00474-17.

1010 40. Amorim R, Temzi A, Griffin BD, Mouland AJ. 2017. Zika virus inhibits eIF2α-dependent
1011 stress granule assembly. PLoS Negl Trop Dis 11:e0005775.

1012 41. Ash PEA, Vanderweyde TE, Youmans KL, Apicco DJ, Wolozin B. 2014. Pathological
1013 stress granules in Alzheimer's disease. Brain Res 1584:52–58.

1014 42. Wang M-D, Gomes J, Cashman NR, Little J, Krewski D. 2014. Intermediate CAG repeat
1015 expansion in the ATXN2 gene is a unique genetic risk factor for ALS--a systematic review
1016 and meta-analysis of observational studies. PLoS One 9:e105534.

1017 43. Pager CT, Schütz S, Abraham TM, Luo G, Sarnow P. 2013. Modulation of hepatitis C
1018 virus RNA abundance and virus release by dispersion of processing bodies and
1019 enrichment of stress granules. Virology 435:472–484.

1020 44. Chen T-C, Hsieh C-H, Sarnow P. 2015. Supporting Role for GTPase Rab27a in Hepatitis
1021 C Virus RNA Replication through a Novel miR-122-Mediated Effect. PLoS Pathog
1022 11:e1005116.

1023 45. Schlegel A, Giddings TH, Ladinsky MS, Kirkegaard K. 1996. Cellular origin and
1024 ultrastructure of membranes induced during poliovirus infection. J Virol 70:6576–6588.

1025 46. Shan C, Xie X, Muruato AE, Rossi SL, Roundy CM, Azar SR, Yang Y, Tesh RB, Bourne
1026 N, Barrett AD, Vasilakis N, Weaver SC, Shi PY. 2016. An Infectious cDNA Clone of Zika
1027 Virus to Study Viral Virulence, Mosquito Transmission, and Antiviral Inhibitors. Cell Host
1028 Microbe 19:891–900.

1029 47. Schwarz MC, Sourisseau M, Espino MM, Gray ES, Chambers MT, Tortorella D, Evans
1030 MJ. 2016. Rescue of the 1947 Zika Virus Prototype Strain with a Cytomegalovirus
1031 Promoter-Driven cDNA Clone. mSphere 1:e00246-16.

1032 48. White JP, Cardenas AM, Marissen WE, Lloyd RE. 2007. Inhibition of Cytoplasmic mRNA
1033 Stress Granule Formation by a Viral Proteinase. Cell Host Microbe 2:295–305.

1034 49. Grant A, Ponia SS, Tripathi S, Balasubramaniam V, Miorin L, Sourisseau M, Schwarz
1035 MC, S??nchez-Seco MP, Evans MJ, Best SM, Garc??a-Sastre A. 2016. Zika Virus
1036 Targets Human STAT2 to Inhibit Type i Interferon Signaling. Cell Host Microbe 19.

1037 50. Donald CL, Brennan B, Cumberworth SL, Rezelj V V., Clark JJ, Cordeiro MT, Freitas de
1038 Oliveira França R, Pena LJ, Wilkie GS, Da Silva Filipe A, Davis C, Hughes J, Varjak M,
1039 Selinger M, Zuvanov L, Owsianka AM, Patel AH, McLauchlan J, Lindenbach BD, Fall G,
1040 Sall AA, Biek R, Rehwinkel J, Schnettler E, Kohl A. 2016. Full Genome Sequence and
1041 sfRNA Interferon Antagonist Activity of Zika Virus from Recife, Brazil. PLoS Negl Trop Dis
1042 10:e0005048.

1043 51. De Maio FA, Risso G, Iglesias NG, Shah P, Pozzi B, Gebhard LG, Mammi P, Mancini E,
1044 Yanovsky MJ, Andino R, Krogan N, Srebrow A, Gamarnik A V. 2016. The Dengue Virus
1045 NS5 Protein Intrudes in the Cellular Spliceosome and Modulates Splicing. PLoS Pathog
1046 12:e1005841.

1047 52. Velázquez-Pérez LC, Rodríguez-Labrada R, Fernandez-Ruiz J. 2017. Spinocerebellar
1048 ataxia type 2: Clinicogenetic aspects, mechanistic insights, and management
1049 approaches. Front Neurol.

1050 53. Nonhoff U, Ralser M, Welzel F, Piccini I, Balzereit D, Yaspo M-L, Lehrach H, Krobitsch S.
1051 2007. Ataxin-2 Interacts with the DEAD/H-Box RNA Helicase DDX6 and Interferes with P-
1052 Bodies and Stress Granules. Mol Biol Cell 18:1385–1396.

1053 54. McIntyre W, Netzband R, Bonenfant G, Biegel JM, Miller C, Fuchs G, Henderson E, Arra
1054 M, Canki M, Fabris D, Pager CT. 2018. Positive-sense RNA viruses reveal the complexity
1055 and dynamics of the cellular and viral epitranscriptomes during infection. Nucleic Acids
1056 Res 46:5776–5791.

1057 55. Huynh DP, Del Bigio MR, Ho DH, Pulst SM. 1999. Expression of ataxin-2 in brains from
1058 normal individuals and patients with Alzheimer's disease and spinocerebellar ataxia 2.
1059 Ann Neurol 45:232–241.

1060 56. Koyano S, Uchihara T, Fujigasaki H, Nakamura A, Yagishita S, Iwabuchi K. 1999.
1061 Neuronal intranuclear inclusions in spinocerebellar ataxia type 2: Triple-labeling
1062 immunofluorescent study. Neurosci Lett.

1063 57. Beck ARP, Medley QG, O'Brien S, Anderson P, Streuli M. 1996. Structure, tissue
1064 distribution and genomic organization of the murine RRM-type RNA binding proteins TIA-
1065 1 and TIAR. Nucleic Acids Res 24:3829–3835.

1066 58. Damgaard CK, Lykke-Andersen J. 2011. Translational coregulation of 5'TOP mRNAs by
1067 TIA-1 and TIAR. Genes Dev 25:2057–2068.

1068 59. Emara MM, Liu H, Davis WG, Brinton M a. 2008. Mutation of mapped TIA-1/TIAR binding
1069 sites in the 3' terminal stem-loop of West Nile virus minus-strand RNA in an infectious
1070 clone negatively affects genomic RNA amplification. J Virol 82:10657–10670.

1071 60. Albornoz A, Carletti T, Corazza G, Marcello A. 2014. The Stress Granule Component
1072 TIA-1 Binds Tick-Borne Encephalitis Virus RNA and Is Recruited to Perinuclear Sites of
1073 Viral Replication To Inhibit Viral Translation. J Virol 88:6611–6622.

1074 61. Apicco DJ, Ash PEA, Maziuk B, LeBlang C, Medalla M, Al Abdullatif A, Ferragud A,
1075 Botelho E, Ballance HI, Dhawan U, Boudeau S, Cruz AL, Kashy D, Wong A, Goldberg
1076 LR, Yazdani N, Zhang C, Ung CY, Tripodis Y, Kanaan NM, Ikezu T, Cottone P, Leszyk J,
1077 Li H, Luebke J, Bryant CD, Wolozin B. 2018. Reducing the RNA binding protein TIA1
1078 protects against tau-mediated neurodegeneration in vivo. Nat Neurosci 21:72–80.

1079 62. Vanderweyde T, Apicco DJJ, Youmans-Kidder K, Ash PEA, Cook C, Lummertz da Rocha
1080 E, Jansen-West K, Frame AAA, Citro A, Leszyk JDD, Ivanov P, Abisambra JFF, Steffen
1081 M, Li H, Petrucelli L, Wolozin B. 2016. Interaction of tau with the RNA-Binding Protein
1082 TIA1 Regulates tau Pathophysiology and Toxicity. Cell Rep 15:1455–1466.

1083 63. Anderson P, Kedersha N. 2008. Stress granules: the Tao of RNA triage. Trends Biochem
1084 Sci 33:141–150.

1085 64. Paranjape SM, Harris E. 2007. Y box-binding protein-1 binds to the dengue virus 3'-
1086 untranslated region and mediates antiviral effects. J Biol Chem 282:30497–30508.

1087 65. Chatel-Chaix L, Melancon P, Racine M-E, Baril M, Lamarre D. 2011. Y-Box-Binding
1088 Protein 1 Interacts with Hepatitis C Virus NS3/4A and Influences the Equilibrium between
1089 Viral RNA Replication and Infectious Particle Production. J Virol 85:11022–11037.

1090 66. Chatel-Chaix L, Germain M-A, Motorina A, Bonneil E, Thibault P, Baril M, Lamarre D.
1091 2013. A Host YB-1 Ribonucleoprotein Complex Is Hijacked by Hepatitis C Virus for the
1092 Control of NS3-Dependent Particle Production. J Virol 87:11704–11720.

1093 67. Aulas A, Caron G, Gkogkas CG, Mohamed N-V, Destroismaisons L, Sonenberg N,
1094 Leclerc N, Parker JA, Vande Velde C. 2015. G3BP1 promotes stress-induced RNA
1095 granule interactions to preserve polyadenylated mRNA. J Cell Biol 209:73–84.

1096 68. Cristea IM, Rozjabek H, Molloy KR, Karki S, White LL, Rice CM, Rout MP, Chait BT,
1097 MacDonald MR. 2010. Host factors associated with the Sindbis virus RNA-dependent
1098 RNA polymerase: role for G3BP1 and G3BP2 in virus replication. J Virol 84:6720–6732.

1099 69. Scholte FEM, Tas A, Albulescu IC, Žusinaite E, Merits A, Snijder EJ, van Hemert MJ.
1100 2015. Stress Granule Components G3BP1 and G3BP2 Play a Proviral Role Early in
1101 Chikungunya Virus Replication. J Virol 89:4457–4469.

1102 70. Fros JJ, Domeradzka NE, Baggen J, Geertsema C, Flipse J, Vlak JM, Pijlman GP. 2012.
1103 Chikungunya Virus nsP3 Blocks Stress Granule Assembly by Recruitment of G3BP into
1104 Cytoplasmic Foci. J Virol 86:10873–10879.

1105 71. Garaigorta U, Heim MH, Boyd B, Wieland S, Chisari F V. 2012. Hepatitis C Virus (HCV)
1106 Induces Formation of Stress Granules Whose Proteins Regulate HCV RNA Replication
1107 and Virus Assembly and Egress. J Virol 86:11043–11056.

1108 72. Yi Z, Pan T, Wu X, Song W, Wang S, Xu Y, Rice CM, Macdonald MR, Yuan Z. 2011.
1109 Hepatitis C virus co-opts Ras-GTPase-activating protein-binding protein 1 for its genome
1110 replication. J Virol 85:6996–7004.

1111 73. Liao K-C, Chuo V, Ng WC, Neo SP, Pompon J, Gunaratne J, Ooi EE, Garcia-Blanco MA.
1112 2018. Identification and characterization of host proteins bound to dengue virus 3′ UTR
1113 reveal an antiviral role for quaking proteins. RNA 24:803–814.

1114 74. Hinman MN, Lou H. 2008. Diverse molecular functions of Hu proteins. Cell Mol Life Sci.

1115 75. Ma WJ, Cheng S, Campbell C, Wright A, Furneaux H. 1996. Cloning and characterization
1116 of HuR, a ubiquitously expressed Elav-like protein. J Biol Chem 271:8144–8151.

1117 76. Tran H, Maurer F, Nagamine Y. 2003. Stabilization of urokinase and urokinase receptor
1118 mRNAs by HuR is linked to its cytoplasmic accumulation induced by activated mitogen-
1119 activated protein kinase-activated protein kinase 2. Mol Cell Biol 23:7177–7188.

1120 77. Dickson AM, Anderson JR, Barnhart MD, Sokoloski KJ, Oko L, Opyrchal M, Galanis E,
1121 Wilusz CJ, Morrison TE, Wilusz J. 2012. Dephosphorylation of HuR Protein during
1122 Alphavirus Infection Is Associated with HuR Relocalization to the Cytoplasm. J Biol Chem
1123 287:36229–36238.

1124 78. Sokoloski KJ, Dickson AM, Chaskey EL, Garneau NL, Wilusz CJ, Wilusz J. 2010. Sindbis
1125 virus usurps the cellular HuR protein to stabilize its transcripts and promote productive
1126 infections in mammalian and mosquito cells. Cell Host Microbe 8:196–207.

1127 79. Rivas-Aravena A, Ramdohr P, Vallejos M, Valiente-Echeverría F, Dormoy-Raclet V,
1128 Rodríguez F, Pino K, Holzmann C, Huidobro-Toro JP, Gallouzi IE, López-Lastra M. 2009.
1129 The Elav-like protein HuR exerts translational control of viral internal ribosome entry sites.
1130 Virology 392:178–185.

1131 80. Barnhart MD, Moon SL, Emch AW, Wilusz CJ, Wilusz J. 2013. Changes in Cellular
1132 mRNA Stability, Splicing, and Polyadenylation through HuR Protein Sequestration by a
1133 Cytoplasmic RNA Virus. Cell Rep 5:909–917.

1134 81. Soto-Acosta R, Xie X, Shan C, Baker CK, Shi P-Y, Rossi SL, Garcia-Blanco MA, Bradrick
1135 S. 2018. Fragile X mental retardation protein is a Zika virus restriction factor that is
1136 antagonized by subgenomic flaviviral RNA. Elife 7.

1137 82. Maziuk B, Ballance HI, Wolozin B. 2017. Dysregulation of RNA Binding Protein

1138 Aggregation in Neurodegenerative Disorders. Front Mol Neurosci 10:89.

1139 83. Wolozin B. 2012. Regulated protein aggregation: stress granules and neurodegeneration.
1140 Mol Neurodegener 7:56.

1141 84. Tang H, Hammack C, Ogden SC, Wen Z, Qian X, Li Y, Yao B, Shin J, Zhang F, Lee EM,
1142 Christian KM, Didier RA, Jin P, Song H, Ming GL. 2016. Zika virus infects human cortical
1143 neural progenitors and attenuates their growth. Cell Stem Cell 18:587–590.

1144 85. Qian X, Nguyen HN, Song MM, Hadiono C, Ogden SC, Hammack C, Yao B, Hamersky
1145 GR, Jacob F, Zhong C, Yoon KJ, Jeang W, Lin L, Li Y, Thakor J, Berg DA, Zhang C,
1146 Kang E, Chickering M, Nauen D, Ho CY, Wen Z, Christian KM, Shi PY, Maher BJ, Wu H,
1147 Jin P, Tang H, Song H, Ming GL. 2016. Brain-Region-Specific Organoids Using Mini-
1148 bioreactors for Modeling ZIKV Exposure. Cell 165:1238–1254.

1149 86. Simonin Y, Loustalot F, Desmetz C, Foulongne V, Constant O, Fournier-Wirth C, Leon F,
1150 Molès J-PP, Goubaud A, Lemaitre J-MM, Maquart M, Leparc-Goffart I, Briant L, Nagot N,
1151 Van de Perre P, Salinas S. 2016. Zika Virus Strains Potentially Display Different
1152 Infectious Profiles in Human Neural Cells. EBioMedicine 12:161–169.

1153 87. Zhang F, Hammack C, Ogden SC, Cheng Y, Lee EM, Wen Z, Qian X, Nguyen HN, Li Y,
1154 Yao B, Xu M, Xu T, Chen L, Wang Z, Feng H, Huang WK, Yoon KJ, Shan C, Huang L,
1155 Qin Z, Christian KM, Shi PY, Xu M, Xia M, Zheng W, Wu H, Song H, Tang H, Ming GL,
1156 Jin P. 2016. Molecular signatures associated with ZIKV exposure in human cortical
1157 neural progenitors. Nucleic Acids Res 44:8610–8620.

1158

1159

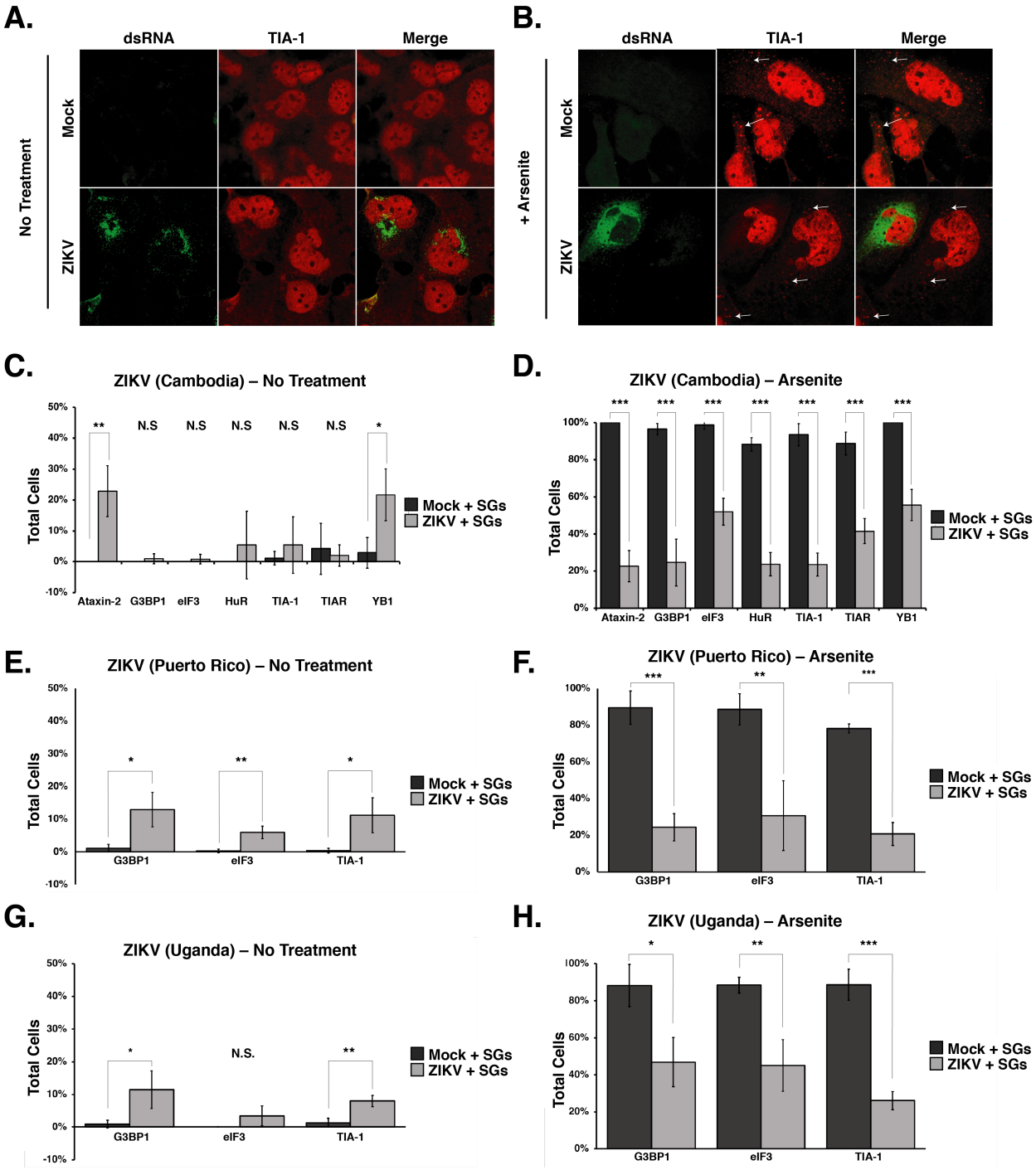

Figure 1. ZIKV restricts the assembly of cellular stress granules. Huh7 cells were either mock-infected or infected with the Cambodia ZIKV-strain (160310) at a MOI of 5. Twenty-four hours post-infection cells were mock-treated or incubated with 5 mM sodium arsenite for 30 minutes, fixed, permeabilized, and analyzed using a 63x oil immersion objective on a Zeiss LSM710 laser scanning confocal microscope. ZIKV-infected cells were detected with mouse-anti-dsRNA antibody (green). The distribution of dsRNA (green) and the stress granule (SG) marker TIA-1 (red) in mock- and ZIKV-infected cells A) not treated and B) treated with sodium arsenite. The white arrows highlight stress granules. Quantification of SGs containing Ataxin-2, G3BP1, eIF3B, HuR, TIA-1, TIAR and YB1 proteins in mock- and ZIKV (Cambodia-

1170 160310)-infected which were either C) not treated or D) treated with sodium arsenite. The number of cells
1171 containing G3BP1, eIF3, and TIA-1-containing SGs in mock-infected cells or cells infected with a Puerto
1172 Rican isolate of ZIKV at a MOI of 5 and either E) not treated or F) treated with sodium arsenite. G-H) SGs
1173 in mock-infected cells and cells infected with the original Ugandan isolate of ZIKV at a MOI of 5 were
1174 quantified. The number of cells containing G3BP1, eIF3, and TIA-1-SG was quantified from cells that were
1175 G) untreated or H) incubated with sodium arsenite. Note, in the original immunofluorescence images, TIA-
1176 1 was visualized using an anti-donkey Alexa Fluor® 647 (magenta) anti-goat IgG secondary antibody. In
1177 panels A) and B) TIA-1 has been pseudo-colored red. The immunofluorescence images are representative
1178 of at least three independent experiments. The errors bars shown on the SG quantification data (Panel 1C,
1179 1D, 1E, 1F, 1G, and 1H) are of the mean ± SD. Significance was determined by two-tailed student T-test
1180 (*$P<0.05$; **$P<0.01$; ***$P<0.001$; and N.S. not significant).
1181

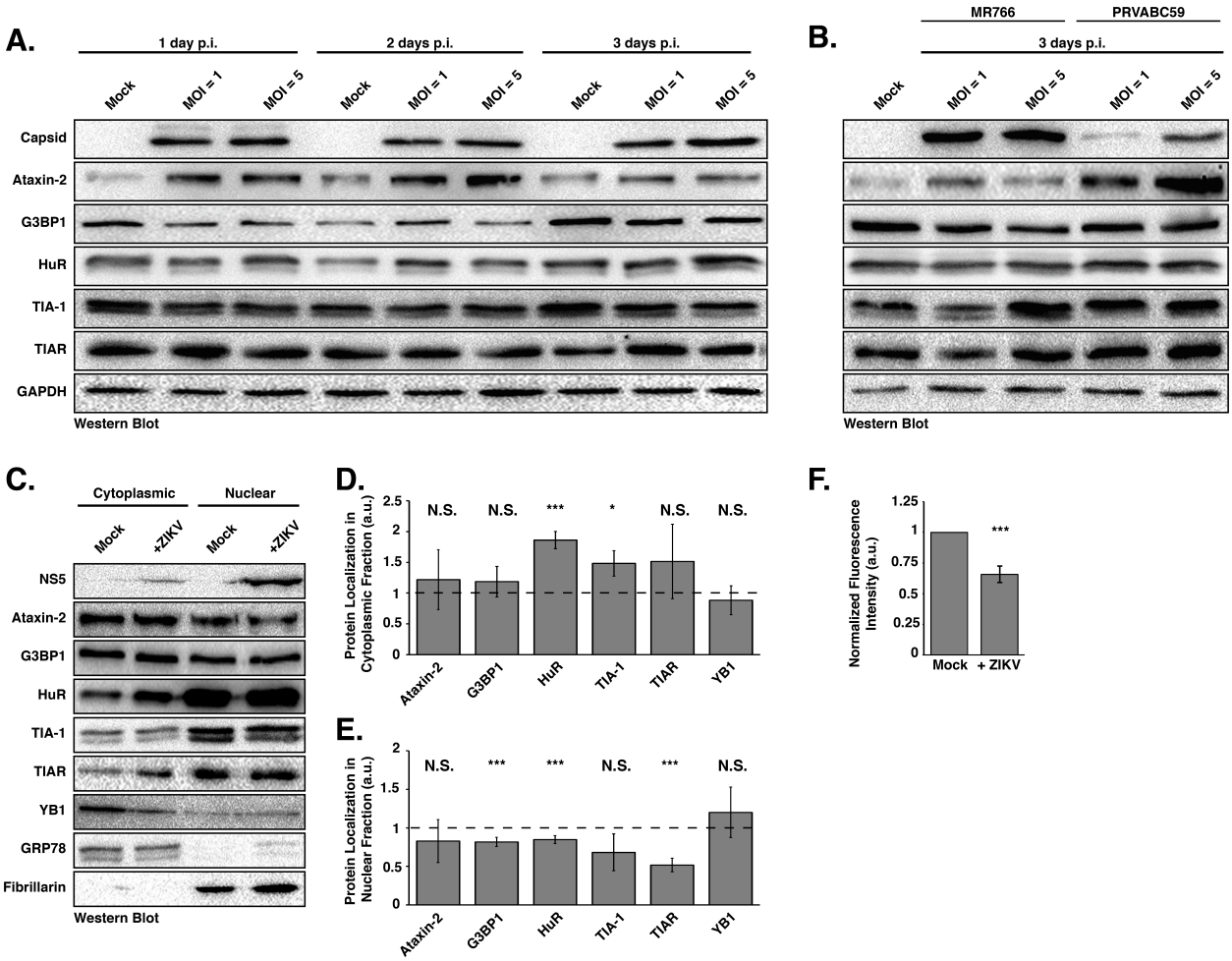

Figure 2. ZIKV infection changes the nuclear and cytoplasmic distribution of stress granule proteins. A) Huh7 cells infected with the Cambodia strain of ZIKV at MOI of 1 or 5 were harvested at 1, 2, and 3 days post-infection. Detection of ZIKV capsid protein by western blot confirmed viral infection. The abundance and integrity of Ataxin-2, G3BP1, HuR, TIA-1 and TIAR proteins was also examined at each time point. The western blot shown is representative of at least three independent experiments. B) Western blot analysis of SG proteins in MR766 and PRVABC59-infected Huh7 cells 3 days post-infection. C) Cytoplasmic and nuclear distribution of Ataxin-2, G3BP1, HuR, TIA-1, TIAR and YB1. Huh7 cells were mock-infected or infected with the Cambodia strain of ZIKV at MOI of 5 and 1-day post-infection the cytoplasmic and nuclear fractions were isolated. The distribution of ZIKV NS5, Ataxin-2, G3BP1, HuR, TIA-1, TIAR, YB1, GRP78 and Fibrillarin was analyzed by western blot. The western blot shown is representative of the three independent experiments performed. Quantification of the distribution of Ataxin-2, G3BP1, HuR, TIA-1, TIAR and YB1 in the D) cytoplasmic and E) nuclear subcellular fractions. The abundance of each SG protein in the cytoplasmic or nuclear fraction was standardized against GRP78 or Fibrillarin, respectively. These values were then normalized against the abundance of the specific SG protein in mock-infected cells, which was assigned the arbitrary unit (a.u.) of one (denoted by dashed line on each graph). The data presented in panels D) and E) were calculated from three independent infections, fractionations and immunoblots. F) Quantification of fluorescence intensity signal of the localization of HuR in the nucleus. Fluorescence intensity was derived in ImageJ using a freehand selection of the nucleus in mock- and ZIKV-infected cells. Values obtained for HuR were divided by the nucleus signal (Hoechst) within mock- and ZIKV-infected cells. Fluorescence intensity of the infected cells were standardized against mock-infected cells and

1205 arbitrarily assigned a value of 1. The relative fluorescence intensity signal was calculated from three
1206 independent experiments and nine cells were counted per experiment. Two-tailed student T-tests were
1207 performed to calculate significance with *P<0.05, ***P<0.001, and N.S. not significant.
1208

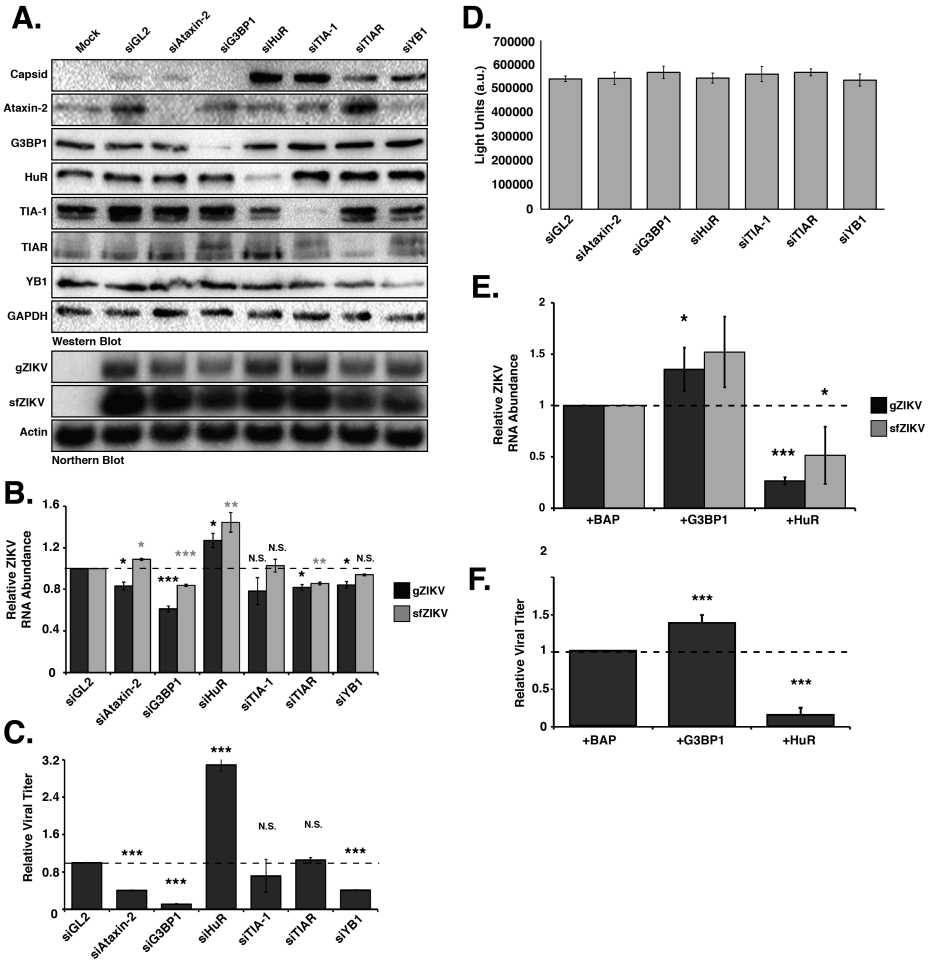

Figure 3. Stress granule proteins promote and limit ZIKV gene expression. Ataxin-2, G3BP1, HuR, TIA-1, TIAR and YB1 proteins were depleted in Huh7 cells using target-specific siRNAs, and then infected 24 hours later at a MOI of 5 with the Cambodia strain of ZIKV (160310). A siRNA targeting *Gaussia* luciferase (siGL2) was used as a control, non-targeting siRNA. Protein, RNA and media were harvested 48 hours post-infection. A) Western blot shows expression of ZIKV capsid, and depletion of each stress granule protein. Expression of GAPDH was used as a loading control, and the western blot shown is representative of at least three independent experiments. The northern blot shows the effect of depleting each stress granule protein on the abundance of the ZIKV genomic (gZIKV) and subgenomic flaviviral (sfZIKV) RNA. Actin mRNA levels were evaluated as a loading control. The northern blot shown is representative of at least three independent experiments. B) Quantification of ZIKV gRNA and sfRNA. ZIKV RNA levels were normalized to actin mRNA, and then represented relative to siGL2 control. C) Viral titers in the extracellular media were determined by plaque assay and relative viral titers were calculated by normalizing titers relative to siGL2 transfected cells. D) A representative assay showing the effect of siRNA depletion of the six SG proteins on cell viability. E) Quantification of ZIKV RNA levels following overexpression of G3BP1-Flag and HuR-Flag. Huh7 cells were transfected with plasmids expressing 3xFlag-Bacterial Alkaline Phosphatase (BAP; control), G3BP1-Flag or HuR-Flag, and then infected with ZIKV (Cambodia-160310) 24 hours post-infection. The effect of overexpressing G3BP1-Flag and HuR-Flag on gZIKV and sfZIKV RNA was evaluated by northern blot. F) Effect of overexpression of G3BP1-Flag and HuR-Flag on viral titers. Data presented in Figure 3 are from at least three independent experiments. Error bars show mean ± SD, and statistical significance was determined using a two-tailed student T-test (*P<0.05; **P<0.01; ***P<0.001; N.S. not significant).

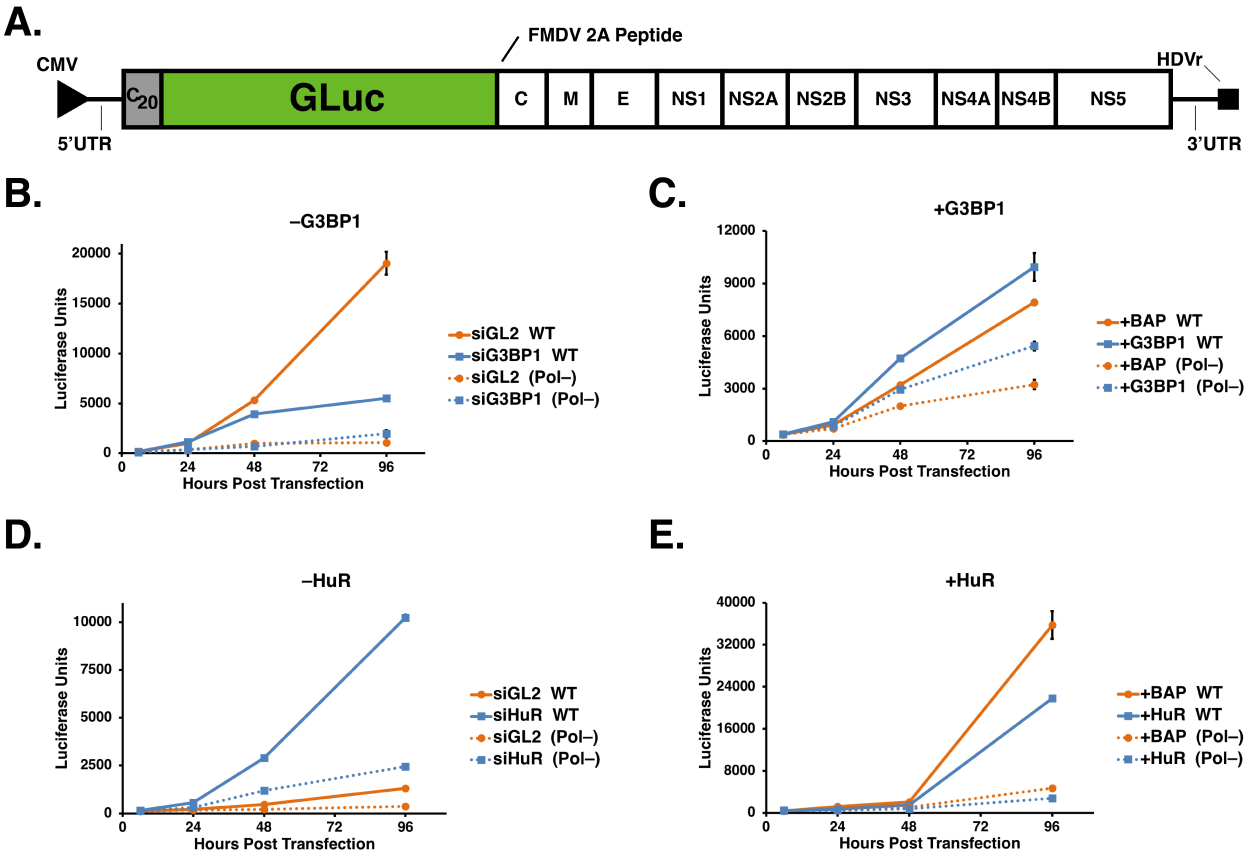

Figure 4. G3BP1 and HuR modulate ZIKV replication. A) Schematic of the ZIKV MR766 *Gaussia* luciferase reporter genome within the pCDNA6.2 MR766 clGLuc Intron3127 HDVr plasmid showing the 5' and 3' UTRs, the mature viral proteins within the single-open reading frame, as well as the position of the *Gaussia* luciferase gene within the MR766 genome. The position of the FMDV 2A peptide within the ZIKV open reading frame, and the two elements within the plasmid namely the CMV promoter and the HDVr, which creates an authentic 3' UTR in the genome, are also denoted. B & D) Huh7 cells were first transfected with either the control or target-specific siRNAs, and then transfected with the same siRNAs and the pCDNA6.2 MR766 clGLuc Intron3127 HDVr WT replication-competent or Pol(-) replication-deficient plasmids. GLuc activity in the media of transfected cells was assayed at 6, 24, 48, and 96 hours post-transfection. C & E) Huh7 cells were transfected with p3xFlag-BAP, pG3BP1-Flag, pHuR-Flag and WT and Pol(-) pCDNA6.2 MR766 clGLuc Intron3127 HDVr. At 6, 24, 48, and 96 hours post-transfection media from the transfected cells was collected and GLuc activity measured. B) Effect of G3BP1 knockdown on ZIKV-GLuc genome expression. C) Effect on ZIKV-GLuc reporter genome expression following overexpression of 3xFlag-BAP (control) and G3BP1-Flag. D) Effect of depleting HuR on ZIKV-GLuc genome expression. E) Effect of overexpressing 3xFlag-BAP and HuR-Flag on ZIKV-GLuc genome expression. The data shown in Figure 4B-4E are from a single experiment and are representative of at least three independent experiments. Error bars indicate mean ± SD.

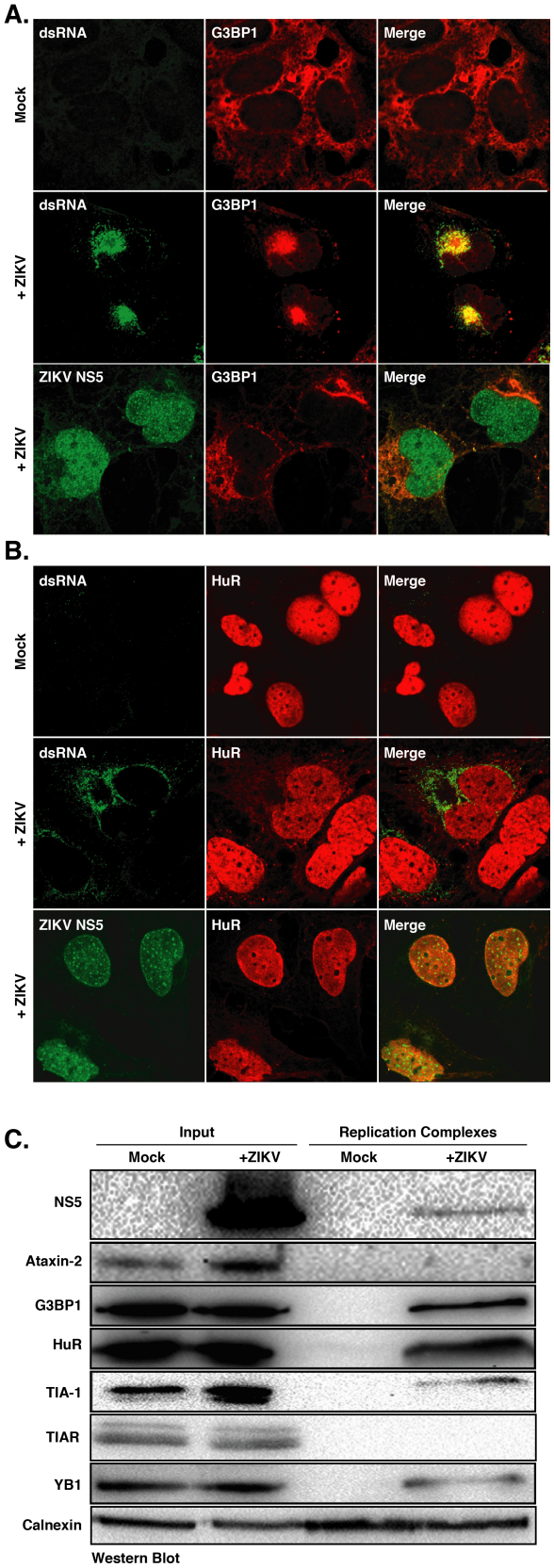
A.
dsRNA
G3BP1
Merge
Mock
dsRNA
G3BP1
Merge
+ ZIKV
ZIKV NS5
G3BP1
Merge
+ ZIKV
B.
dsRNA
HuR
Merge
Mock
dsRNA
HuR
Merge
+ ZIKV
ZIKV NS5
HuR
Merge
+ ZIKV
C.
Input
Replication Complexes
Mock
+ZIKV
Mock
+ZIKV
NS5
Ataxin-2
G3BP1
HuR
TIA-1
TIAR
YB1
Calnexin
Western Blot

1253

1254 **Figure 5. G3BP1 and HuR localize with ZIKV replication complexes.** A-B) Huh7 cells were either mock-
1255 infected or infected with the Cambodia ZIKV strain at a MOI of 5. One day post-infection cells were fixed,
1256 permeabilized, and prepared for confocal imaging. Immunofluorescence images are representative of at
1257 least three independent experiments. A) Immunofluorescence image showing G3BP1 (red) localization in
1258 mock- infected cells and with viral replication sites as visualized by the staining with antibodies to dsRNA
1259 and NS5 (green) in ZIKV-infected cells. B) Localization of HuR (red) in mock-infected cells and with dsRNA
1260 and NS5 (green) in ZIKV-infected cells. C) Western blot analysis of ZIKV NS5, Ataxin-2, G3BP1, HuR, TIA-
1261 1, TIAR, YB1, and calnexin associated with replication complexes isolated from mock- and ZIKV-infected
1262 Huh7 cells. The western blot is representative of three independent experiments.
1263
1264

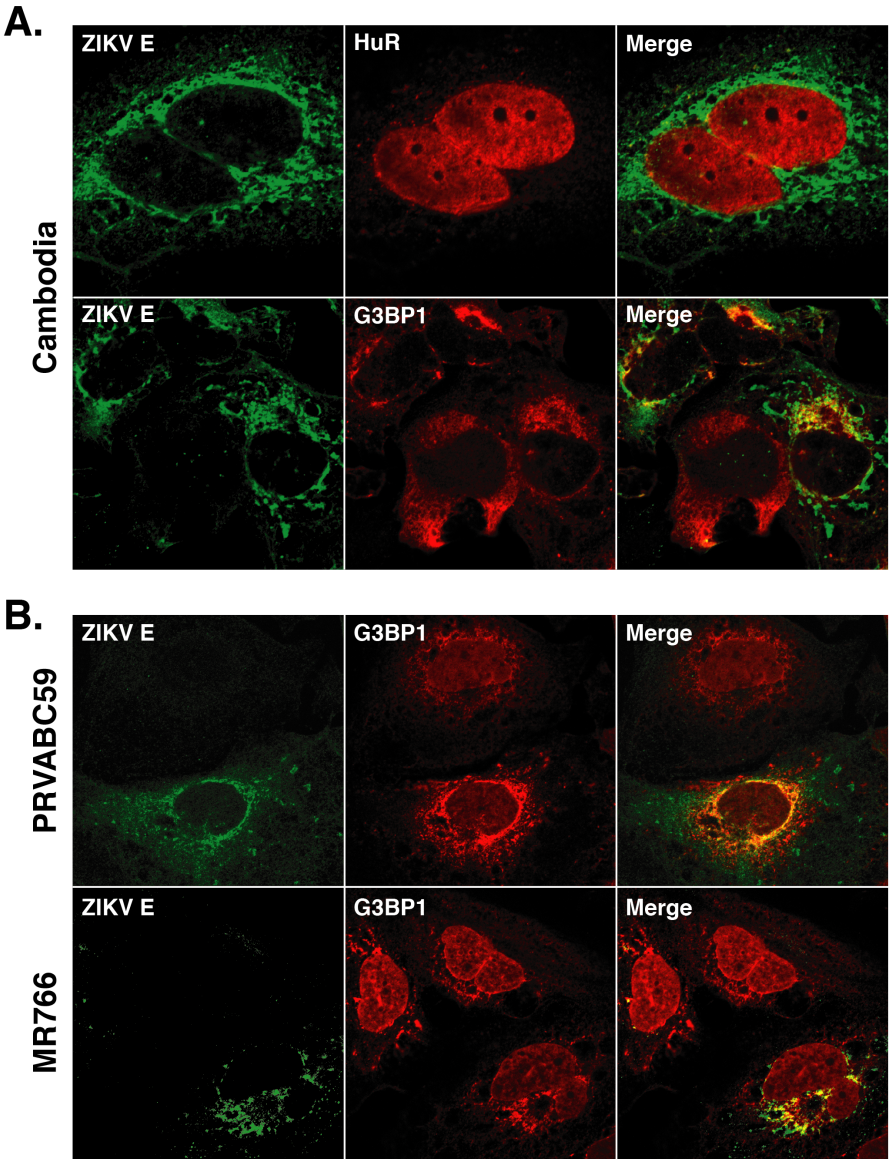

1265
1266
1267 **Figure 6. G3BP1 co-localizes with ZIKV E protein.** One day post-infection Huh7 cells infected with ZIKV
1268 at a MOI of 5 were fixed, permeabilized, and prepared for confocal imaging. A) Localization of ZIKV E
1269 protein with HuR and G3BP1 following infection with the Cambodia strain of ZIKV. B) Localization of ZIKV
1270 E protein with G3BP1 following infection with the Puerto Rican (PRVABC59) and Ugandan (MR766) strains
1271 of ZIKV, respectively. The immunofluorescence images shown are representative of at least three
1272 independent experiments.